Review Article

Nano Research
2023, 16(1): 1338–1361

ISSN 1998-0124 CN 11-5974/O4
https://doi.org/10.1007/s12274-022-4682-y

Advanced MOF-based electrode materials for supercapacitors and electrocatalytic oxygen reduction

Bolong Yang[1,§], Bingjie Li[2,§] (✉), and Zhonghua Xiang[1] (✉)

[1] *State Key Laboratory of Organic-Inorganic Composites, Beijing University of Chemical Technology, Beijing 100029, China*
[2] *The First Affiliated Hospital of Zhengzhou University, Zhengzhou 450052, China*
[§] *Bolong Yang and Bingjie Li contributed equally to this work.*

Received: 13 May 2022 / **Revised:** 12 June 2022 / **Accepted:** 20 June 2022

ABSTRACT

Metal-organic frameworks (MOFs) have attracted a lot of attention due to their diverse structures, favorable porous properties, and tunable chemical compositions in the multiple fields. Notably, MOF-based materials (including pristine MOFs, MOF composites, and their derivatives) play the vital role in electrochemical energy storage and conversion systems, due to their ability for regulating chemical composition at the molecular level and their highly porous frameworks for facilitating the mass and charge transfer. Supercapacitors and fuel cells are used as one of energy storage and conversion systems respectively, and it is unstoppable to design and synthesize high-efficiency electrode materials for them. This review starts with the strategies for designing targeted MOF-based materials in electrochemical energy storage and conversion applications followed by the state-of-the-art MOF-based materials discussed as to their potential applications in supercapacitors and electrocatalytic oxygen reduction reaction (ORR). Finally, the challenges and perspectives of MOF-based materials applied for supercapacitors and electrocatalytic ORR are discussed.

KEYWORDS

metal-organic frameworks (MOFs), MOF composites, MOF derivatives, supercapacitors, electrocatalytic oxygen reduction reaction (ORR)

1 Introduction

Since the industrial revolution, a large amount of fossil fuels have been consumed to promote economic development and brought unprecedented prosperity to human society [1, 2]. The combustion of these fuels will inevitably emit a massive amount of carbon dioxide, which is considered the main greenhouse gas leading to global warming [3, 4]. The comprehensive strategy to address climate change is to build a clean, low-carbon, safe, and efficient energy system by improving the utilization of renewable and environmentally friendly energy sources and storage devices, to achieve carbon neutralization as soon as possible [5, 6]. Electrochemical energy storage and conversion technologies have been recognized as the most practical choice to alleviate the increasingly serious energy crisis and environmental damage due to their high energy conversion efficiency and low environmental pollution [7, 8]. As a result, efforts are being made to promote sustainable energy storage and conversion systems, such as supercapacitors and fuel cells. The former is the main energy storage system, in which advanced electrode materials with high specific capacitance (SC) and durability are highly desired [9, 10]. The latter is the main energy conversion system, in which functional electrocatalysts with high activity and stability are essential [11]. Although the working principles of these electrochemical systems are different, they all have the similar pursuit for the physicochemical properties of materials, such as high specific surface area (SSA), good electrical conductivity, hierarchical porous structure, excellent electrocatalytic activity and selectivity, and long-term stability, which determines their ultimate storage capacity and conversion efficiency in electrochemical energy storage and conversion devices [12, 13]. Therefore, looking for new functional materials with ideal composition and structure has always been the top priority of future electrochemical energy storage and conversion technology.

Metal-organic frameworks (MOFs) are a class of crystalline porous polymers with periodic network structures formed by metal ions (or metal clusters) and organic ligands. MOFs are considered one of the best links between nanotechnology and energy storage due to their high specific surface area, abundant pores, controllable morphology, and multi-functionalities [14–16]. Up to now, more than 20,000 MOFs with diverse crystal structures, compositions, and morphologies have been discovered and this number is still increasing. Several MOFs have been directly used as electrode materials for supercapacitors and electrocatalytic oxygen reduction reaction (ORR) [17]. The use of pristine MOFs with high surface area and the large diversity of metal ions as electrode materials for supercapacitors shows great potential and advantages. When using pure MOFs as electrode materials, low chemical stability and lack of electrical conductivity are the two key problems that have to face. So some MOFs are also used as supports to composite with active nanomaterials to solve above problems, including the combination of MOF and carbon materials (active carbon (AC), carbon nanotubes (CNTs),

Address correspondence to Bingjie Li, bingjie.li@monash.edu; Zhonghua Xiang, xiangzh@mail.buct.edu.cn

and graphene), conductive polymers, metal doping, and so on. Additionally, various nanostructured derivatives were obtained by calcination using MOFs as sacrificial templates for supercapacitors and ORR. [18, 19]. Compared with traditional porous materials, these MOF derived materials have some unique advantages, such as controllable morphology, and carbon-based materials have higher specific surface area and conductivity, regular structure, heteroatom *in situ* doping, and so on. In conclusion, MOF-based nanomaterials show great potential in the field of supercapacitors and electrocatalytic ORR due to their unique properties.

In this review, we systematically summarize the recent advances of pure MOFs, MOF composites, and their derivatives as electrode materials for supercapacitors and electrocatalytic ORR. Recent breakthroughs in MOF-based electrode materials are highlighted with an emphasis on synthesis strategy, morphology/structural control, component manipulation, and electrochemical performance evaluation (Fig. 1). Finally, this review summarizes the major current challenges along with some solutions and potential development trends of MOFs as electrode materials for supercapacitors and electrocatalytic ORR. We believe that this review will stimulate extensive interest to further accelerate and explore the innovations of MOF-based materials in the field of electrochemical energy storage and conversion.

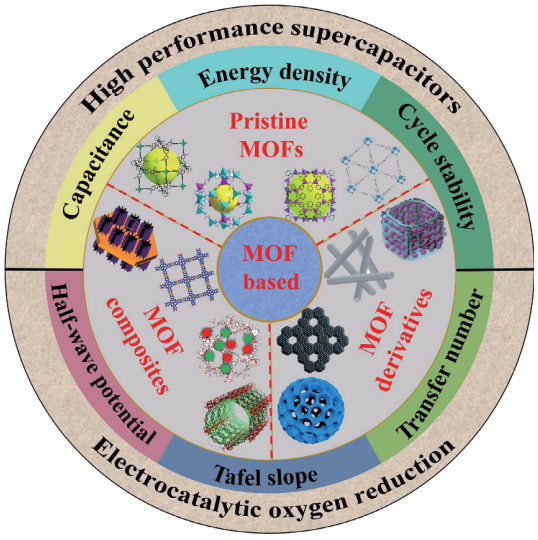

Figure 1 Overview of pristine MOFs, MOF composites, and MOF derivatives for supercapacitors and electrocatalytic oxygen reduction applications.

2 Strategies for synthesis of MOFs and their derived materials

MOFs are a new type of porous crystal materials formed by the coordination of bridging organic ligands with metal centers, which have been extensively studied in the field of electrochemistry due to their large specific surface area, tunable structure, and high porosity.

2.1 Pristine MOFs

In general, aromatic carboxylic acids, such as 5-methylisophthalic acid and 2-(2,5-dicarboxylphenyl) nicotinic acid, and nitrogen-containing heterocycles, such as imidazole and bipyridine, are used as ligands to connect metal centers [20, 21]. The most commonly used methods for the synthesis of MOFs are hydrothermal and solvothermal. For example, Li et al. [22]. have synthesized a novel Cu-MOF with two-dimensional (2D) (4,4) layers by the assembly of Cu^{II} ion and bib under the $CH_3OH/CHCl_3$ system. The as-prepared Cu-MOF sample shows a hierarchically stacking nanosheet with interspace, which is well matched with the 2D intrinsic feature. In the classical solution-based MOF formation process, nano porous materials are firstly formed through nucleation and diffusion processes, and then multiple nucleation and surface adsorbed organic molecules polymerize to form inorganic–organic crystals. To prepare controllable MOFs crystals in a short time, some alternative synthesis methods have been tried, such as microwave heating, ultrasonic treatment, electrochemical deposition, and mechanochemical methods (Fig. 2) [23–25]. For example, Kim et al. [26] have prepared a UiO-66(Zr)-$(OH)_2$ MOF containing defects using a microwave-assisted continuous-flow tubular reactor following our previous procedure. There are many factors affecting the structure of MOFs, such as metal ions, anions, organic ligands, and solvents [27–30]. As shown in Fig. 3, it can be clearly seen that factors such as metal ions, anions, organic ligands, solvents, etc. will cause significant changes in the crystal structure of MOFs. Therefore, the target MOF material can be designed and prepared purposefully by adjusting these parameters. In fact, the structure and functional properties of MOFs are the result of the interaction of these factors, and it is due to a variety of synthetic factors that a wide range of MOFs are brewed. In order to meet the wide application of MOFs in the energy field, single MOFs, bimetallic MOFs, and core–shell MOFs have been continuously developed. In most cases, MOFs crystals have microporous properties that can be controlled between angstroms and

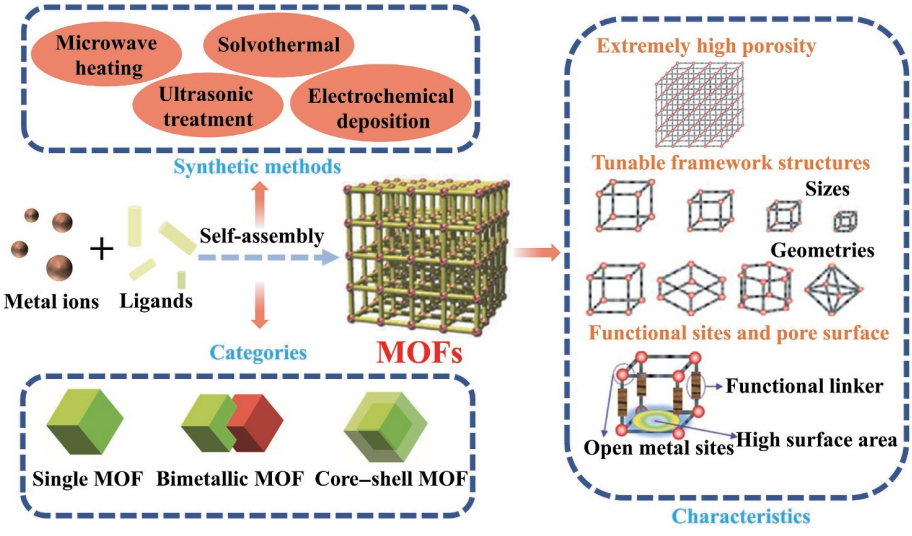

Figure 2 Schematic illustration of controlled synthesis of MOFs.

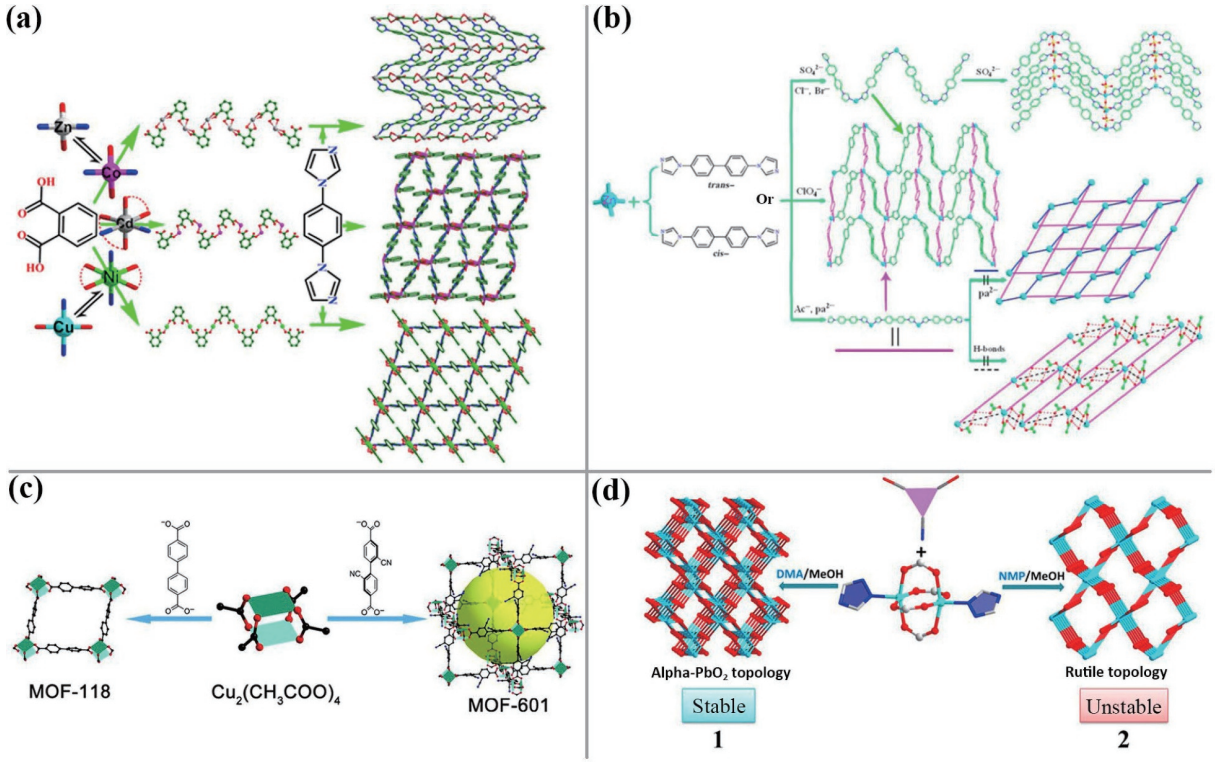

Figure 3 Effects of (a) metal ions, (b) anions, (c) organic ligands, and (d) solvents on the structure of MOFs. (a) Reprinted with permission from Ref. [27], © American Chemical Society 2018. (b) Reprinted with permission from Ref. [28], © Elsevier Inc. 2015. (c) Reprinted with permission from Ref. [29], © American Chemical Society 2008. (d) Reprinted with permission from Ref. [30], © American Chemical Society 2011.

nanometers depending on the actual application to the materials. Additionally, MOFs also have the advantages of tunable framework structures, open metal sites, and controllable morphology. It is precisely because of these characteristics that the application value of MOF materials in the field of energy field has been continuously explored in the past two decades.

2.2 MOF composites

There are two main problems in the used MOFs process: lack of chemical stability and electrical conductivity. To overcome the shortcomings of pristine MOFs and expand its application range, MOF composites have been synthesized and studied. These MOF composites not only exhibit high electrical conductivity, but also possess strong chemical stability (Fig. 4). It is worth noting that the synergistic effect of the interaction between components and structures makes these composites possess new physical/chemical properties, resulting in great activity and stability. For example, MOFs will be combined with conductive components such as polyaniline (PANI), graphene oxide, CNT, and so on [31–34]. For example, Sanko et al. [35] prepared a magnetite MOF@CNT nanohybrid material to enhance pores structure hydrothermally for electrochemical detection of adenine and guanine purine bases. Wang et al. [36] fabricated nano-hybrids (MOF@GO) with intumescent fire retardants by the incorporation of bimetallic MOF and graphene oxide (GO). Moreover, MOF composites can be divided into 0D, 1D, 2D, and 3D materials by dimensionality. Each component in the MOF-based composite materials has its own unique function, which can overcome the defects of a single counterpart, produce a synergistic effect, and improve the properties of composites.

2.3 MOF derivatives

Additionally, to synthesize an ideal electrode material, some important factors need to be considered, such as simplicity,

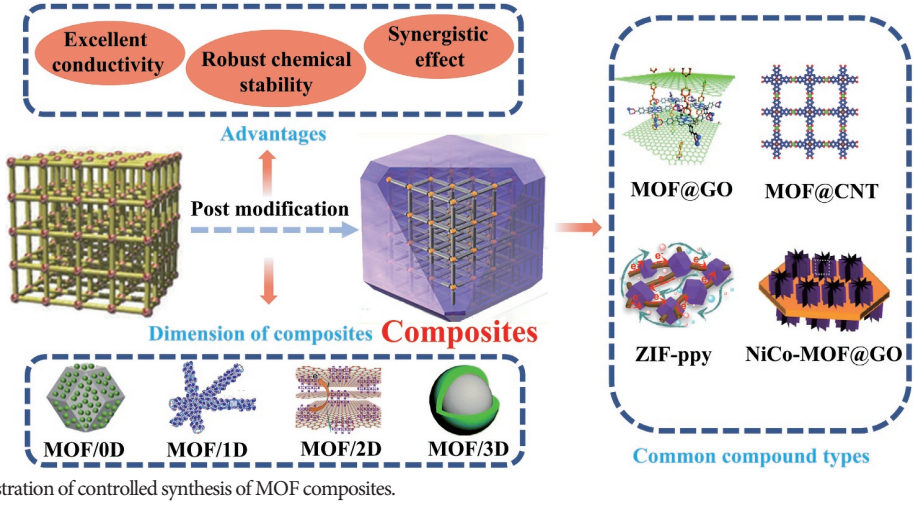

Figure 4 Schematic illustration of controlled synthesis of MOF composites.

rapidity, durability, large number of active sites, specific surface area, porosity, good conductivity, and appropriate cost. Due to their unique composition and topological structure, MOFs are used to prepared many materials, such as nanostructured carbon, metallic compounds, as well as metallic compound/carbon hybrids. Since the thermal and chemical instability of MOFs may hinder their direct application, various methods are employed to control the calcination pyrolysis process without additional templates or complex procedures, so it has significant advantages over traditional methods. In the pyrolysis process, the calcination atmosphere often includes Ar_2, N_2, NH_3, H_2, S, P, etc. (Fig. 5). These gases are widely used as inert protective gases or heteroatom-doped raw materials. Modulating the structure of MOFs by means of defect, surface modification, heterostructure, and support interaction to obtain MOF derivatives with excellent electrochemical performance has been widely concerned. Due to the diversity of MOFs, MOF precursors with different morphologies can be prepared, which often maintain the original morphology after high-temperature pyrolysis. Therefore, by designing and synthesizing the morphology of structures such as hierarchical, yolk–shell, porous, triple-shell, frame, hollow, etc., the pore structure of the material can be changed, thereby accelerating the electrochemical reaction. Metal/carbon matrix composites were prepared by *in-situ* carbonization of MOF-based precursors in an inert atmosphere [37]. The resulting nanomaterials usually show a porous structure and retain the original morphology of MOF particles. In addition, various metal based compounds, including sulfides, phosphides, and selenides, can through the introduction of heteroatom functional groups such as sulfur, phosphorus, and selenium into organic ligands get corresponding heteroatom doping MOF materials accompanying with the subsequent one-step calcination [38]. On the other hand, they can be obtained by reacting MOF-based templates with corresponding gas/vapor [39]. More importantly, the structure and characteristics of MOF derived materials strongly depend on the initial properties of MOF precursors, which indicates that the electrode materials with novel structure and excellent electrochemical performance can be obtained by fully mastering various complex factors in the preparation process of MOFs and their derivatives, instead of using the "hit or fail" method.

3 MOFs for supercapacitors

Emerging as a new type of porous materials, MOFs are promising electrode materials for supercapacitors due to their advantages of large surface areas, adjustable pore sizes, and incorporated redox metal centers.

3.1 Energy storage mechanisms in supercapacitors

Electrochemical capacitors, also known as supercapacitors with long cycle stability, well operational safety, high power density (PD), and good electrochemical reversibility have attracted great attention. Supercapacitors are widely used in the national economy, science, technology, and daily life [40, 41]. According to the charge storage mechanism, supercapacitors can be divided into three types of capacitance behavior: (1) Electrochemical double layer capacitors (EDLC) use the pure electrostatic charge accumulation at the electrode interface, in which the electrode materials usually employ carbon-based active materials with high surface areas, including carbon nanotube, micro/mesoporous carbon, graphene, and so on [42]. (2) Pseudo-capacitance developed from fast and reversible surface redox processes at characteristic potentials. Transition metal oxides/sulfides and conducting polymers are representative examples of electrode materials on pseudo-capacitors (Fig. 6). (3) Hybrid capacitors take advantage of both mechanisms.

Figure 7 shows the schematic diagram (cyclic voltammetry (CV)) and corresponding galvanostatic charge–discharge (GCD) curves of capacitive, pseudocapacitive, and battery type electrode materials [43]. In response to potential scanning, EDLCs usually

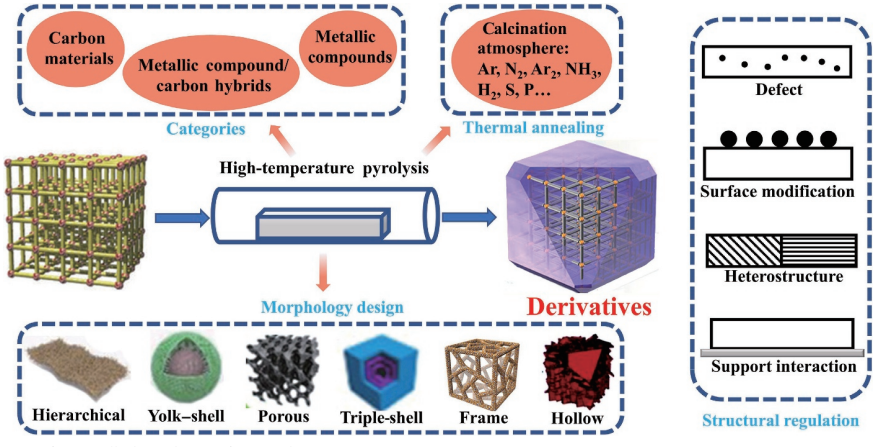

Figure 5 Schematic illustration of controlled synthesis of MOF derivatives.

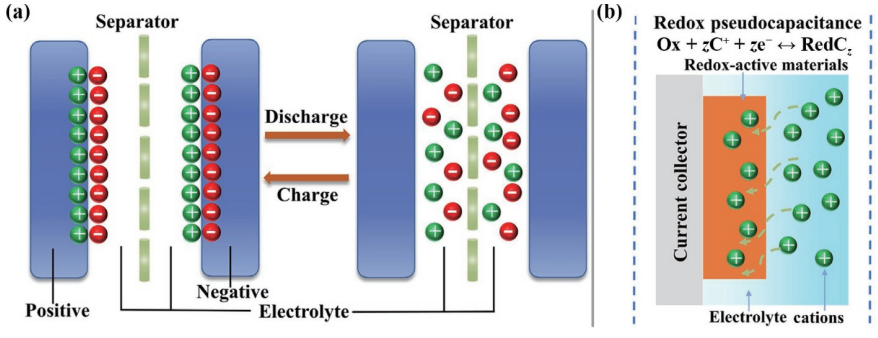

Figure 6 Schematics of charge-storage mechanisms for (a) an EDLC and (b) pseudocapacitive electrodes.

exhibited a potential-independent capacitance. Therefore, the CV curves of supercapacitors often remained a rectangular shape, and the current was almost constant during charge/discharge processes (Figs. 7(a) and 7(b)). On the other hand, while the battery type electrode materials were selected for potential scanning, the CV curves displayed separated oxidation and reduction peaks with significant Faradaic reactions (Figs. 7(g) and 7(h)). The GCD profiles of EDLCs showed a sloping shape with a constant slope value (Fig. 7(c)). In comparison, the E versus t plot for battery-type material was nonlinear and exhibited a relatively flat charge/discharge plateau at a constant voltage stage (Fig. 7(i)). These two extreme signals in CV curves suggest pseudo-capacitance behaviour (Figs. 7(d)–7(f)). As shown in Figs. 7(b), 7(d), and 7(e), pseudocapacitive materials include surface redox, intercalation-type and intercalation-type, with a wide range of reversible redox materials.

Recently, MOF-based materials as electrode materials for supercapacitors have been extensively developed. On the one hand, the capacitances generated by MOF-derived porous carbon materials in supercapacitors belong to the double-layer capacitance reaction mechanism. On the other hand, the capacitances contributed by other MOF-based materials belong to the pseudo-capacitance reaction mechanism. Moreover, carbon materials and other MOF-based materials can be assembled into hybrid capacitors by using them as positive and negative electrodes respectively.

3.2 Pristine MOFs for supercapacitors

The use of pristine MOFs with high surface area and large diversity of metal ions as electrode materials for supercapacitors shows great potential and advantages. Díaz et al. [44] reported the Co8-MOF-5 materials. Electrical conductivity and stability of Co8-MOF-5 were good enough at this stage while its electrochemical performance was limited by the particular MOF and the electrolyte used. A 2D Co-based layered MOF, Co-LMOF, has been synthesized and has introduced as a novel electrode material for supercapacitors [45]. The Co-LMOF exhibited higher specific capacitance and excellent cycling stability in 1 M KOH. Additionally, a range of 23 different MOF compounds with different metals and organic ligands have been synthesized [46]. It was found that a zirconium-based MOF showed the highest stack and areal performance and well stability. These findings constitute an important step in adopting the abundant MOFs chemistry for the development of high-capacitance supercapacitors in the future.

Bimetallic MOFs could provide richer redox reactions deriving from improved charge transfer between different metal ions [47]. A 2D Co/Ni-MOF nanoflakes have been synthesized by the hydrothermal method [48]. The 2D M-MOFs exhibited preeminent electrochemical performance and cycling stability, which is attributed to the favorable paths for ions diffusion (Figs. 8(a)–8(c)). Naderi et al. [49] synthesizes a Ni/Co-based bimetallic MOF and evaluated its energy storage performance. The Ni/Co-MOF showed excellent capacitance of 1,023 $F{\cdot}g^{-1}$ at the scan rate (SR) of 2 $mV{\cdot}s^{-1}$ and excellent stability (Figs. 8(d)–8(g)). The low electrical conductivity and the unique microporous structure greatly limited the possibility for MOFs to fabricate high-performance electrodes of supercapacitors. To overcome these shortcomings, Gao et al. [50] successfully prepared hierarchical porous Zr-MOFs. The as-assembled supercapacitors exhibited a high energy density (ED) of 32 $Wh{\cdot}kg^{-1}$ at a power density of 240 $W{\cdot}kg^{-1}$ (Fig. 8(h)). Dinca et al. [51] synthesized a $Ni_3(HITP)_2$-MOF with high electrical conductivity, which can serve as the sole electrode material in an EDLC (Fig. 8(i)). The MOF-based device exhibited a good capacitance and capacity retention greater than 90% after 10,000 cycles. Very recently, Li et al. [52] reported the fabrication of conductive MOF nanowire arrays (NWAs). The Cu-CAT NWAs in solid-state supercapacitors showed excellent areal capacitance (22 $\mu F{\cdot}cm^{-2}$) and good rate performance (Figs. 8(j)–8(l)).

3.3 MOF composites for supercapacitors

When using pure MOFs as electrode materials for supercapacitors, low chemical stability and lack of electrical conductivity are the two key problems that have to solve. MOF composites have been utilized as electrode materials to solve the above problems, including the combination of MOF and carbon materials (AC,

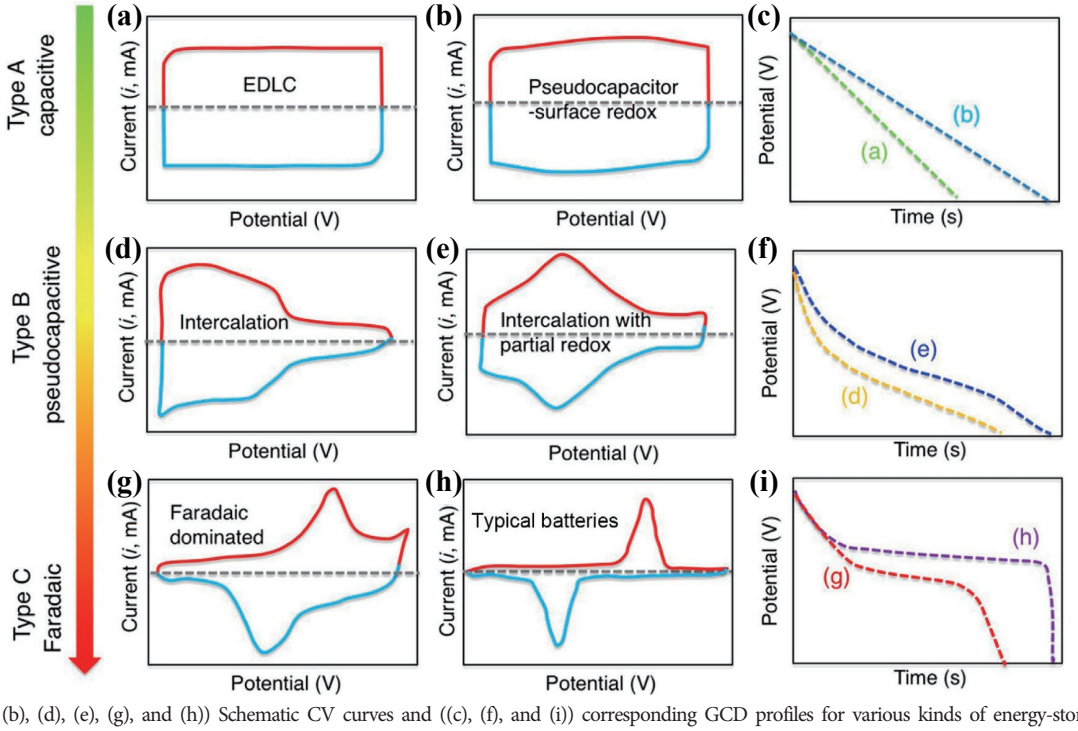

Figure 7 ((a), (b), (d), (e), (g), and (h)) Schematic CV curves and ((c), (f), and (i)) corresponding GCD profiles for various kinds of energy-storage materials. Reprinted with permission from Ref. [43], © American Chemical Society 2018.

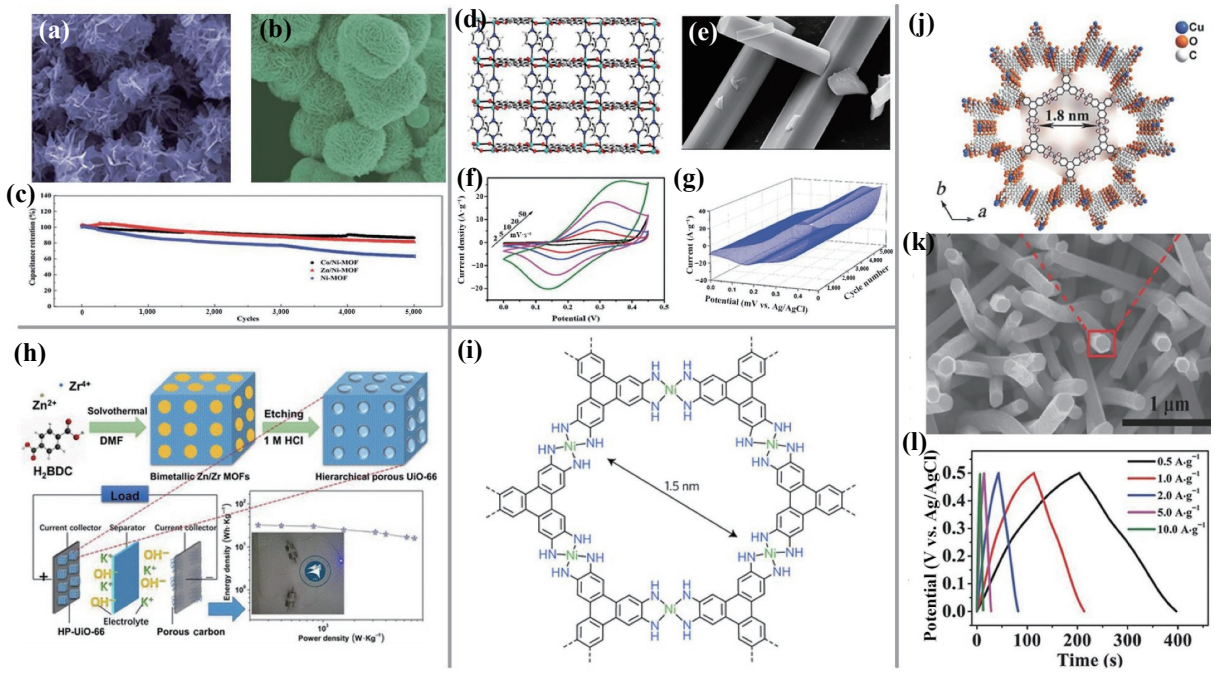

Figure 8 Pristine MOFs for supercapacitors. Scanning electron microscopy (SEM) images of the as-synthesized (a) Co/Ni-MOF and (b) Zn/Ni-MOF. (c) Cycling performance. Reprinted with permission from Ref. [48], © The Royal Society of Chemistry 2017. (d) Perspective view of the 3D framework in Ni/Co-MOF along *b* axis. (e) Field emission SEM (FESEM) images of Ni/Co-MOF. (f) Cyclic voltammogram with different scan rates. (g) 3D-CCV curves of the Ni/Co-MOF electrode measured at the scan rate of 100 mV·s^{-1}. Reprinted with permission from Ref. [49], © The Royal Society of Chemistry 2016. (h) Schematic synthesis of the HP-UiO-66 and schematic of PC//HP-UiO-66 asymmetric supercapacitor (ASC). Reprinted with permission from Ref. [50], © American Chemical Society 2017. (i) Molecular structure of conductive $Ni_3(HITP)_2$. Reprinted with permission from Ref. [51], © Macmillan Publishers Limited, part of Springer Nature 2016. (j) Crystal structure of Cu-CAT viewed along the *c*-axis. (k) SEM image of the Cu-CAT NWAs growing on carbon fiber paper. (l) Galvanostatic charge and discharge curves at different current densities. Reprinted with permission from Ref. [52], © WILEY-VCH Verlag GmbH & Co. KGaA, Weinheim 2017.

CNTs, and graphene), conductive polymers, metal doping, and so on [53, 54].

Mousavi et al. [55] reported a Ni/Co-MOF material, which exhibited a high specific capacitance of 860 F·g^{-1} at the current density (CD) of 1.0 A·g^{-1}. (Fig. 9(a)). By manipulating the particle size of MOF-based electrode active materials, a facile one-pot co-synthesis method was used to *in situ* prepare uniformly distributed MOF particles at the nanoscale level, opening a new pathway for obtaining MOF composites with excellent supercapacitive properties. A bimetallic MOF (Ni-Co-MOF) was directly grown on the surface of graphene oxide sheets (Ni-Co-MOF/GO) and used as a hybrid supercapacitor electrode (Fig. 9(b)) [56], exhibiting the maximum specific capacitance of 447.2 F·g^{-1} at a current density of 1 A·g^{-1} and excellent rate capability (Figs. 9(c) and 9(d)). The Ni-Co-MOF/GO material is expected to be applied as a high-performance supercapacitor electrode material. The composite of rGO-HKUST-1 has been prepared by an ultrasonication mixing method and used as the supercapacitor electrode material [57]. The electrode exhibited a high specific capacitance (Figs. 9(e)–9(g)). Moreover, a novel and multitasking Cu-MOF/rGO hybrid has been prepared by a facile ultra-sonication assisted method (Fig. 9(h)) [58]. Due to the positive synergistic effects between Cu-MOF crystals and rGO nanosheets, the Cu-MOF/rGO hybrid showed high charge storage efficiency, high energy, and excellent rate ability (retained 71.01% of its initial capacitance at 8 A·g^{-1}). In addition to carbon materials, MOF combined with conducting polymers has also been researched as electrode for supercapacitors. Wang et al. [59] demonstrated a strategy to construct a flexible MOF-based supercapacitor, by interweaving Co-MOF crystals that were coated on carbon cloth with electrochemically polymerized PANI (Fig. 10(a)). Guo et al. [60] synthesized carbonized MOF-PANI composite by a novel and facile route. The synthetic process for the sandwich-like carbonized Zn-MOF/PANI composites is shown in Fig. 10(b), which shows excellent electrochemical performance (Figs. 10(c) and 10(d)). After carbonization, the conductivity of the active material was improved, and the ability of PANI storage electrolyte and electrochemical activity were enhanced. Chen et al. [61] incorporated conductive polypyrrole (PPy) into the bimetal-organic framework, and constructed high performance electrode materials (Zn/Ni-MOF@PPy; Fig. 10(e)). Lu et al. [62] grew MOF nanosheets on electrospun polyacrylonitrile (PAN) nanofibers (PPNF@MOF) and applied them as supercapacitor electrode materials, which exhibited a high capacitance of 702.8 F·g^{-1} at 0.5 A·g^{-1} and excellent cycling stabilities (Fig. 10(f)). Xu et al. [63] demonstrated a general and effective strategy to synthesize a flexible MOFs-based supercapacitor device via using preprepared PPy tubes as the support for *in situ* growth of MOF particles (Figs. 10(g)–10(i)). The obtained zeolitic imidazolate framework (ZIF)-PPy-2 exhibited continuous microstructures, which increases electron transfer between the MOF particles and maintains a high effective porosity of the MOF. It is worth noting that the synergistic effect of the interaction between components and structures makes these composites possess new physical/chemical properties that are not present in the single components, resulting in great activity and stability [64, 65].

3.4 MOF derivatives for supercapacitors

In comparison to the attempts to explore pure MOFs and MOF composites for supercapacitors, there is an increasing trend of utilizing them as pyrolysis precursors/self-sacrificing templates to synthesize MOF derivatives with controllable morphology, size, and composition. Compared with traditional porous materials, these MOF derived materials have the following unique advantages. 1) The morphology, size, structure, and other features inherited from the MOFs can be effectively retained; 2) the existence of organic ligands in MOFs provides advantages for the

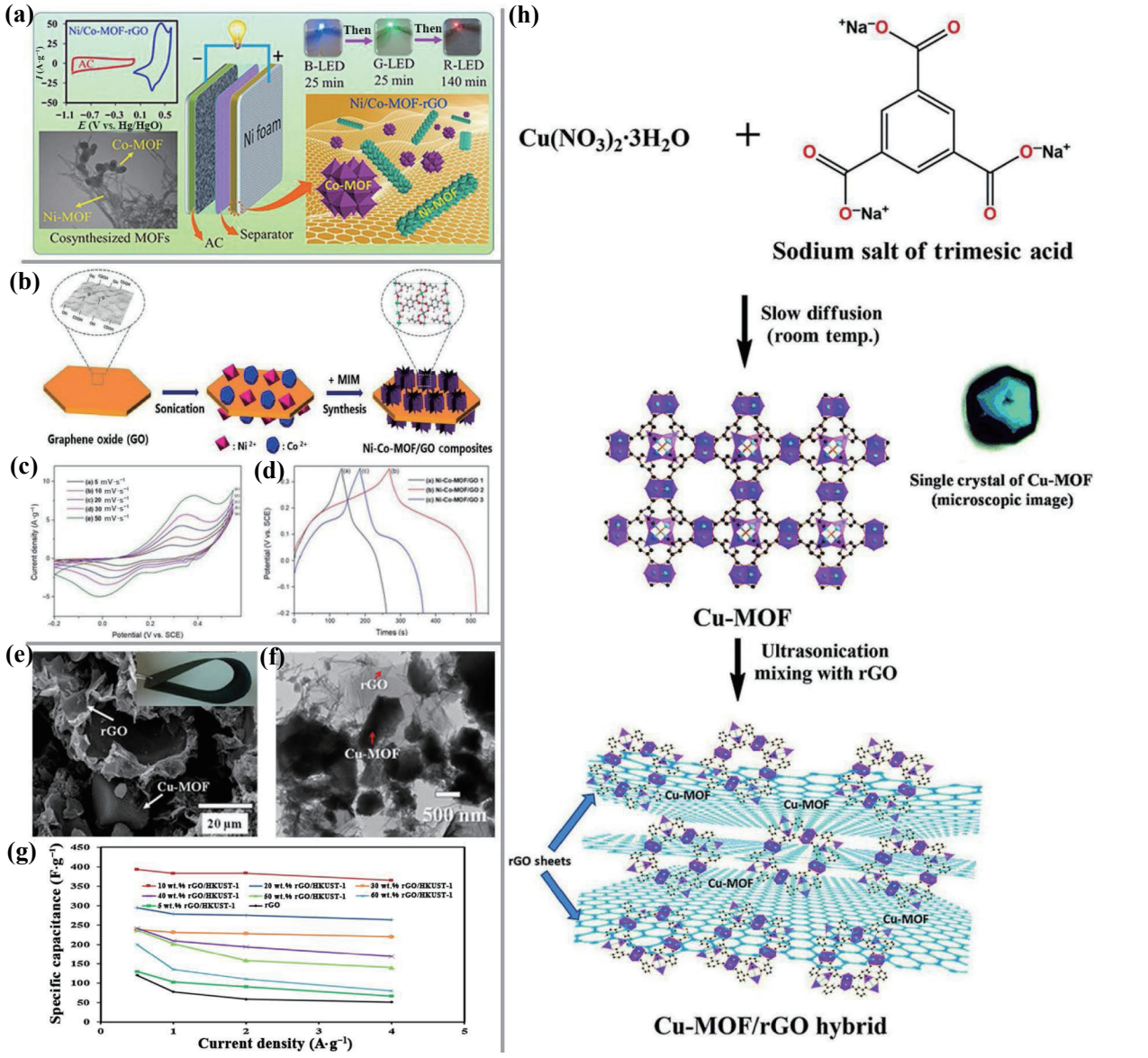

Figure 9 MOF composites for supercapacitors. (a) Schematic of AC//Ni/Co-MOF-rGO ASC and electrochemical properties. Reprinted with permission from Ref. [55], © Elsevier Ltd. 2018. (b) Preparation process diagram for Ni-Co-MOF/GO composites. (c) CV plots and (d) GCD results of Ni-Co-MOF/GO composites in 6 M KOH. Reprinted with permission from Ref. [56], © Elsevier Ltd. 2019. (e) and (f) SEM and transmission electron microscopy (TEM) images of rGO-HKUST-1 composite. (g) The specific capacitances vs. applied current densities at different loading contents of rGO. Reprinted with permission from Ref. [57], © Elsevier Ltd. 2015. (h) Schematic synthesis of Cu-MOF. Reprinted with permission from Ref. [58], © The Royal Society of Chemistry 2016.

formation of carbon-based materials, and the resulting carbon matrix has higher specific surface area and conductivity, which accelerates the charge transfer process; 3) the regular structure of the MOF makes the metal components and carbon evenly distributed and prevents their further agglomeration and sintering, which is impossible to achieve by simple mixing of the carbon with the materials; 4) various heteroatoms (N, O, C, P, and so on) can provide more active sites and higher electrical conductivity, thus improving the electrochemical performance [66–68]. According to the different chemical compositions, we divide these derivatives into the following three categories.

3.4.1 *Carbon materials for supercapacitors*

Porous carbons with high surface area and optimized pore size distributions are the most widely used electrode materials for supercapacitors. Xu's group [69] first reported zinc-based M-HPNCs (Fig. 11(a)). In the process of carbonization, organic components were pyrolyzed, leaving a porous carbon backbone, and zinc ions evaporated in the form of zinc vapor, leaving more holes (boiling point of Zn: 907 °C). After calculation, the specific capacitance was 204 F·g^{-1} at scan rate of 0.5 mV·s^{-1} (Figs. 11(b) and 11(c)). Wang et al. [70] constructed "brick-and-mortar" sandwiched porous carbon and the as-assembled symmetric supercapacitor can deliver a high energy density (Fig. 11(d)). Salunkhe et al. [71] have designed novel symmetric supercapacitors based on nitrogen-doped porous by direct carbonization of ZIF-8 without using an additional precursor (Fig. 11(e)). The nanoporous carbon (NPC) materials exhibited excellent electrochemical performance with a maximum specific capacitance of 251 F·g^{-1} at 5 mV·s^{-1}. Xu's group [72] have prepared porous carbon materials with high specific surface areas and good electrochemical performances by using a robust N-containing MOF (ZIF-8) as the precursor and furfuryl alcohol as the other precursor via an easily handled method (Fig. 11(f)). The pore structure and surface area of the resultant carbon materials can be tuned simply by changing the calcination temperature (Fig. 11(g)). The obtained NPC displayed a specific capacitance up to 188 F·g^{-1} at the scan rate of 5 mV·s^{-1} (Fig. 11(h)). As displayed in Fig. 11(i), composites of 3D hollow carbon sphere from lotus pollen (HPNCs/CS) were prepared by facile carbonization of ZIF-8 [73].

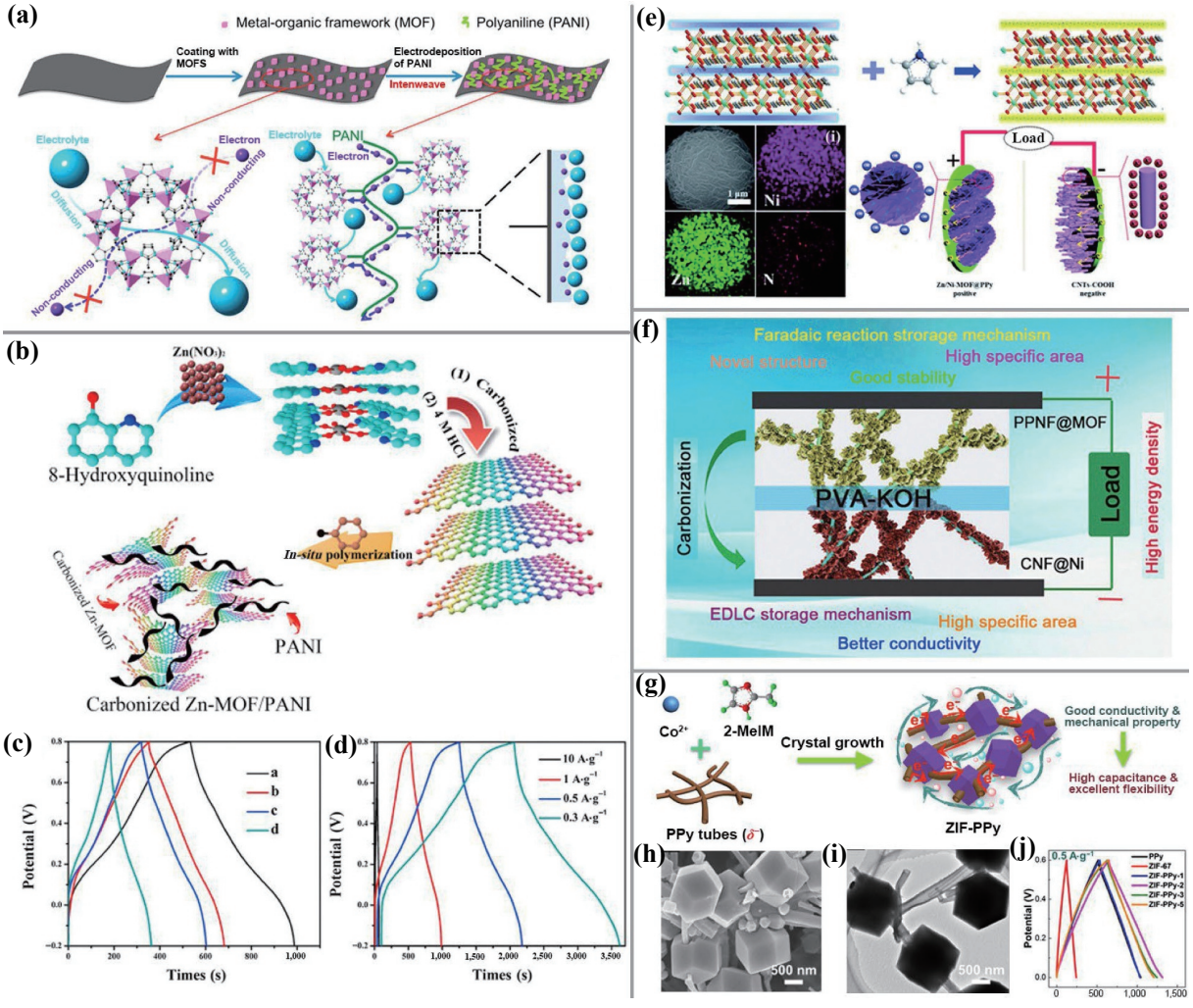

Figure 10 MOF composites for supercapacitors. (a) The construct for PANI-ZIF-67-CC and the schematic representation of electron and electrolyte conduction in MOF and MOF interwoven by PANI. Reprinted with permission from Ref. [59], © American Chemical Society 2015. (b) Schematic illustration of synthesizing sandwich structure of carbonized Zn-MOF/PANI composites. (c) Glvanostatic charge discharge curves at 1 $A·g^{-1}$. (d) Galvanostatic charge discharge curves of ZMP-0.04. Reprinted with permission from Ref. [60], © Elsevier B.V. 2016. (e) Schematic illustration of pyrrole polymerization occurring in the Zn/Ni-MOF. Reprinted with permission from Ref. [61], © The Royal Society of Chemistry 2017. (f) Schematic sketch of the flexible solid-state PPNF@MOF (anode)//CNF@Ni (cathode) ASC. Reprinted with permission from Ref. [62], © Elsevier B.V. 2018. (g) A schematic of the preparation of ZIF-PPy. (h) and (i) FESEM and TEM images of ZIF-PPy-2. (j) GCD profiles at 0.5 $A·g^{-1}$ of PPy, ZIF-67, and ZIF-PPy hybrids. Reprinted with permission from Ref. [63], © American Chemical Society 2017.

The obtained sample exhibited a high specific capacitance and excellent cycle stability (Figs. 11(j) and 11(k)). Yu et al. [74] reported a facile strategy for generating bimodal porosity in porous carbons by using a sacrificed ZIF-8 as the precursor and additional silica colloids as extra progenies via further self-assembly (Fig. 11(l)). This new concept provides a direction for the design and synthesis of multi-layer porous carbon materials to improve the electrochemical performance of supercapacitor electrodes. Another kind of NPC material was synthesized by controlled carbonization of bimetallic Co/Zn-ZIF at 800 °C and then oxidation at 250–300 °C (Fig. 12(g)) [75]. Bimetallic Co_x-$Zn_{1-x}(MeIm)_2$ has been successfully synthesized due to the crystal compatibility between ZIF-8 and ZIF-67 (Fig. 12(e)) [76]. Zinc ions play a role in pore formation, while organic ligands connected with cobalt ions often produce graphite carbon after carbonization, which is due to the catalytic graphitization effect controlled by cobalt nanoparticles. This study provides a practical way to obtain carbon materials with excellent properties by adjusting the components of the bimetallic ZIFs. Moreover, Zhu et al. [77] presented the fabrication of N and S co-doped carbon nano capsules from a MOF composite by a facile and effective external template-free method (Fig. 12(f)), which exhibited hierarchical porosity and superior supercapacitor performance. One- and two-dimensional carbon nanomaterials are widely concerned due to their excellent thermal mechanical and electrical properties and have broad application prospects. The process of synthesizing these materials is often quite complex and consumes a lot of energy, so it is a great challenge to develop simple and effective methods to prepare these materials. Recently, Xu's group [78] developed facile and effective methods for the preparation of 1D carbon nanorods and 2D graphene nanoribbons (Fig. 12(a)). These materials had excellent electrochemical properties of supercapacitors (Figs. 12(b)–12(d)). Su et al. [79] successfully obtained the mesoporous carbon hexagonal-nanodisks via catalytic carbonization of nonporous Fe-based coordination polymers, which showed excellent electrochemical performance for EDLCs (Fig. 12(h)). Additionally, the performance of many MOF-derived carbon materials in supercapacitors is shown in Table 1.

3.4.2 *Metallic compounds for supercapacitors*

The metal compounds derived from MOFs have the advantages of good porosity, adjustable or controllable chemical composition and morphology. These unique characteristics can increase the capacity, improve the electrical conductivity, and enhance the stability, which makes MOF derived metal compounds have a

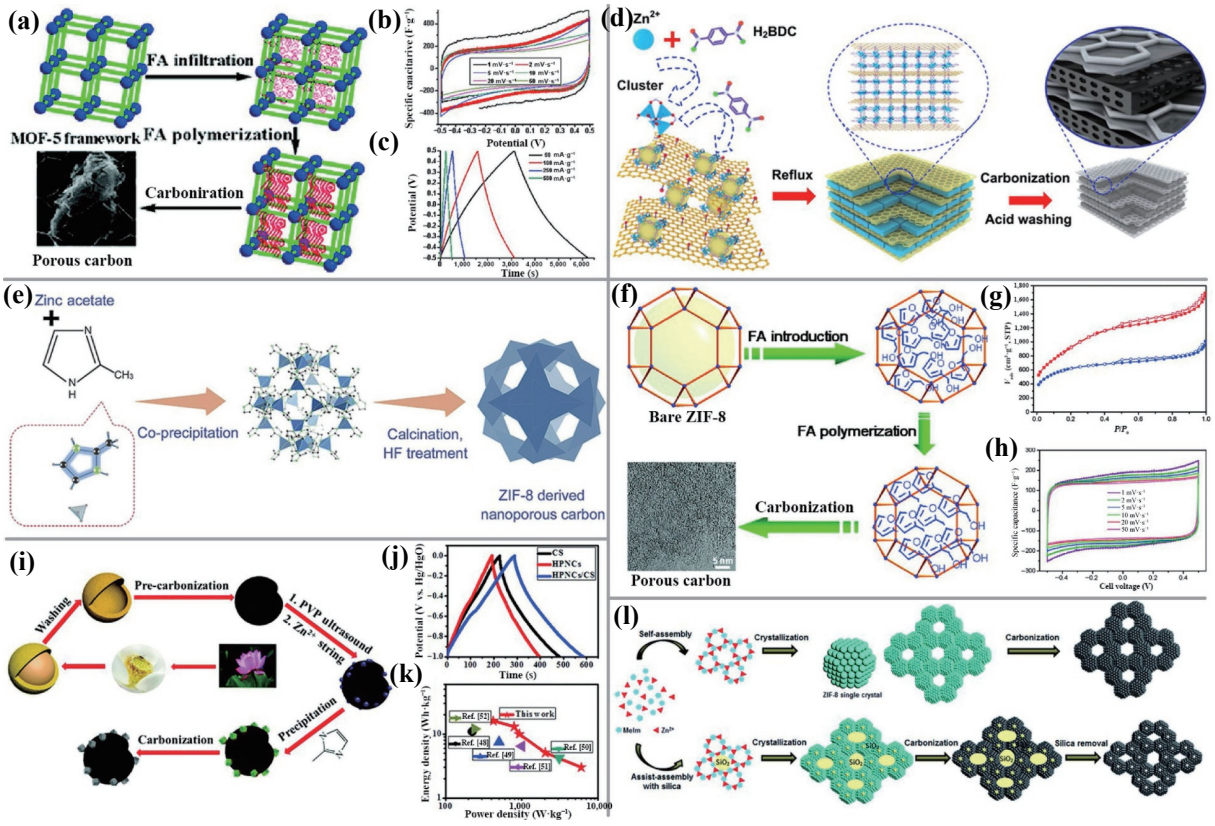

Figure 11 MOF derived carbon materials for supercapacitors. (a) Schematic illustration of synthesizing porous carbon. (b) Cyclic voltammograms. (c) galvanostatic charge/discharge. Reprinted with permission from Ref. [69], © American Chemical Society 2008. (d) Schematic illustration showing the fabrication process for porous carbon building using MOFs and graphene oxide as precursors. Reprinted with permission from Ref. [70], © Elsevier Ltd. 2016. (e) Schematic illustration of synthesis of NPC materials derived from MOFs. Reprinted with permission from Ref. [71], © The Royal Society of Chemistry 2014. (f) Schematic illustration of the preparation procedure for nanoporous carbon. (g) Nitrogen adsorption–desorption isotherms. (h) CVs at different scan rates for C1000 samples. Reprinted with permission from Ref. [72], © American Chemical Society 2011. (i) Schematic illustration of the approach to fabricating hierarchical interpenetrating 3D hollow HPNCs/CS composite. (j) GCD curves tested at 1 A·g^{-1}. (k) Ragone plot of HPNCs/CS//HPNCs/CS. Reprinted with permission from Ref. [73], © The Royal Society of Chemistry 2017. (l) Formation process of porous carbons with bimodal porosity via self and assisted assembly approaches. Reprinted with permission from Ref. [74], © The Royal Society of Chemistry 2014.

great prospect of application as electrode materials for supercapacitors [88]. The utilization of MOFs as precursors for the preparation of metal oxides has many advantages, such as high specific surface area, abundant pores, and flexible chemical composition. Generally, porous metal oxides can be obtained by simply heat treatment of MOF precursors in air. For example, a porous Co_3O_4 aggregate has been obtained by the simple thermolysis of Co-MOF crystals [89]. Apart from metal oxides, MOF-derived metal hydroxides were also investigated as electrode materials. Normally, metal hydroxides have been obtained by hydrothermal/solvothermal treatment of MOFs. Qu et al. [90] introduced a simple hydrothermal procedure to fabricate highly porous MOF-74-derived Ni-Co bimetallic hydroxides (denoted as MDH) (Figs. 13(a)–13(c)). The 65Ni-MDH was used as positive materials to assemble asymmetric supercapacitors, and the maximum energy density of 81 Wh·kg^{-1} with a power density of 1.9 kW·kg^{-1} was realized. Similarly, Zhang et al. [91] fabricated a hollow Ni-Co layered double hydroxide by using ZIF-67 as the self-sacrificial template and cobalt precursor (Fig. 13(d)).

Additionally, sulfides and phosphides have also attracted more and more interest for their high porosity and abundant active sites. As shown in Fig. 13(e), Hu and coworkers [92] reported template-engaged formation of double-shelled hollow nanostructures CoS-NP/CoS-NS DSNBs as advanced electrodes for supercapacitors by use of the unique reactivity of yolk–shell structured ZIF-67. Ma et al. [93] reported a simple and convenient route to synthesize NiS hierarchical hollow cubic structures by an anion exchange reaction (Fig. 13(f)). The NiS hierarchical hollow cubes exhibited large specific capacitance and well cycling stability.

Apart from sulfides, MOF-derived phosphides also demonstrate promising electrode materials. Liang et al. [94] presented a MOF-based strategy to synthesize NiCo-P hollow nanocage as a electrode material for supercapacitor (Fig. 13(g)). As a battery-type Faradaic electrode material for fast energy storage, NiCo-P hollow nanocage had a high specific capacity of 894 C·g^{-1} at 1 A·g^{-1} and good rate capability.

3.4.3 *Metallic compound/carbon hybrids for supercapacitors*

Although metallic compounds have high specific capacitances, there are still some major drawbacks in the use of supercapacitor electrode materials due to their poor conductivity, low electrode surface area, and short cycle life [95, 96]. Carbon loaded metallic compound materials have better stability compared to pure metallic oxide materials in the application of supercapacitors, because the carbon matrix can effectively reduce the mechanical stress due to the synergies effect of pseudo capacitance materials and EDLC materials [97].

Carbon materials@metal oxide electrode materials have attracted significant interest for supercapacitors. Wang et al. [98] developed a novel ASC based on carbon nanotubes@nickel oxide nanosheets (CNT@NiO) core–shell composites and porous carbon polyhedrons (PCPs) as the positive and negative electrodes respectively (Figs. 14(a) and 14(b)). The as-prepared ASC exhibited a high energy density and excellent stability (Fig. 14(c)). Additionally, a Mn_2O_3/3-D graphene network (3DGN) hybrid derived from Mn-BTC/3DGN has shown remarkable electrochemical performance for free-standing supercapacitors

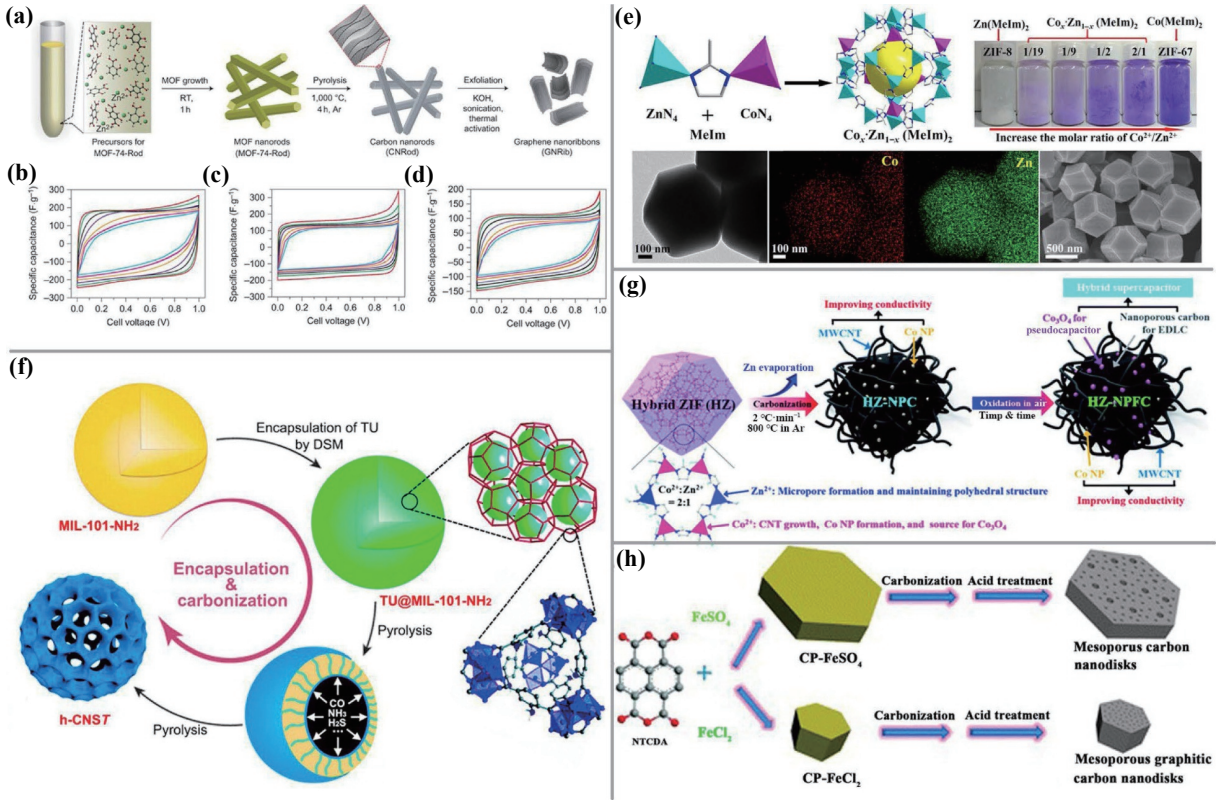

Figure 12 MOF derived carbon materials for supercapacitors. (a) Scheme of synthesis of MOF-74-Rod, carbon nanorods, and graphene nanoribbons. Cyclic voltammograms at different sweep rates using (b) graphene nanoribbons, (c) carbon nanorods, and (d) microporous carbon (MPC) as electrode materials. Reprinted with permission from Ref. [78], © Macmillan Publishers Limited 2016. (e) Schematic illustration of the crystal structure and the bimetallic ZIF (Co_x·Zn_{1-x}(MeIm)$_2$) crystals as well as TEM and SEM images of the $Co_{0.1}$·$Zn_{0.9}$(MeIm)$_2$. Reprinted with permission from Ref. [76], © Tang, J. et al. 2016. (f) Schematic representation of the encapsulation of thiourea (TU) into MIL-101-NH_2 by a double-solvent method (DSM) and subsequent formation of the N and S co-doped hollow cellular carbon nanocapsules. Reprinted with permission from Ref. [77], © Elsevier B.V. 2017. (g) Representation of the nanoarchitecture design for the functional MOF-derived nanoporous carbon, hybrid ZIF-derived nanoporous functional composites (HZ-NPFC) from the Co^{2+}/Zn^{2+} hybrid ZIF obtained. Reprinted with permission from Ref. [75], © The Royal Society of Chemistry 2017. (h) Schematic illustration for the synthesis of mesoporous carbon nanodisks via direct carbonization of coordination polymers. Reprinted with permission from Ref. [79], © The Royal Society of Chemistry 2012.

Table 1 MOF-derived carbon materials for supercapacitors

Electrode materials	Electrolyte	SSA (m^2·g^{-1})	SR (mV·s^{-1})/CD (A·g^{-1})	SC (F·g^{-1})	ED (Wh·Kg^{-1})	PD (W·Kg^{-1})
ZIF-8 derived carbon [80]	1 M H_2SO_4	1,140	1 A·g^{-1}	86	23.5	700
ZIF-67 derived nanoporous carbon [81]	1 M H_2SO_4	—	1 A·g^{-1}	75	60	1,200
ZIF-67 derived porous carbon [82]	6 M KOH	—	1 A·g^{-1}	101	34	775
ZIF-8 derived polyhedral porous carbon [83]	1 M $LiPF_6$	3,680.6	—	—	155	200
MOF derived carbon [84]	2 M KOH	998	1 A·g^{-1}	161	47.1	1,018
NPMOF-700 [85]	6 M KOH	381	1 A·g^{-1}	220	4.5	1,000
N-NFC[a] [86]	1 M H_2SO_4	277.2	1 A·g^{-1}	387.3	7.9	219
LIC-(MOF-199@ZIF-67)-based MSCs[b] [87]	1 M H_2SO_4	210	1 mV·s^{-1}	1.9	—	—

[a]N-NFC: nitrogen-doped nanofibrous carbon; [b]MSCs: micro-supercapacitors.

(Fig. 14(d)) [99]. The designed 3DGN/Mn_2O_3 electrode material showed a high specific capacitance of 471.1 F·g^{-1} at 0.2 A·g^{-1}, well rate capability, and excellent long-cycle stability (Figs. 14(e) and 14(f)). Wang et al. [100] successfully synthesized a series of porous mixed metal/metal oxide@carbon materials (M/MO@C) samples by the direct carbonization of CoMn-MOF-74 (Fig. 14(g)). M/MO@C exhibits excellent electrochemical performance when assembled into asymmetric supercapacitors as negative materials. (Figs. 14(h)–14(j)). Furthermore, Tong et al. [101] successfully synthesized 2D Co/Ni MOFs nanosheets@S,N-doped carbon composites (2D CoNi@SNC) derived from 2D Co/Ni MOFs with a surface area of 224 m^2·g^{-1}, a porous structure, and good conductivity (Figs. 14(k)–14(m)).

For the synthesis of most MOF derivatives, two basic strategies are usually used to control the chemical composition: (1) regulating the composition of MOF precursors; (2) manipulating conversion factors. Of course, these two strategies are often used simultaneously in many cases to obtain excellent electrochemical performance. Due to the diversity of MOF and its transformation processes, these MOF derived materials are often protean and have good electrochemical properties. However, the synthesis of MOF derivatives is still in its infancy stage, and the performance of supercapacitors needs to be further improved [102, 103]. Therefore, the relationship between the physicochemical properties of the materials and their electrocatalytic performance should be reflected in the design and construction of these MOF

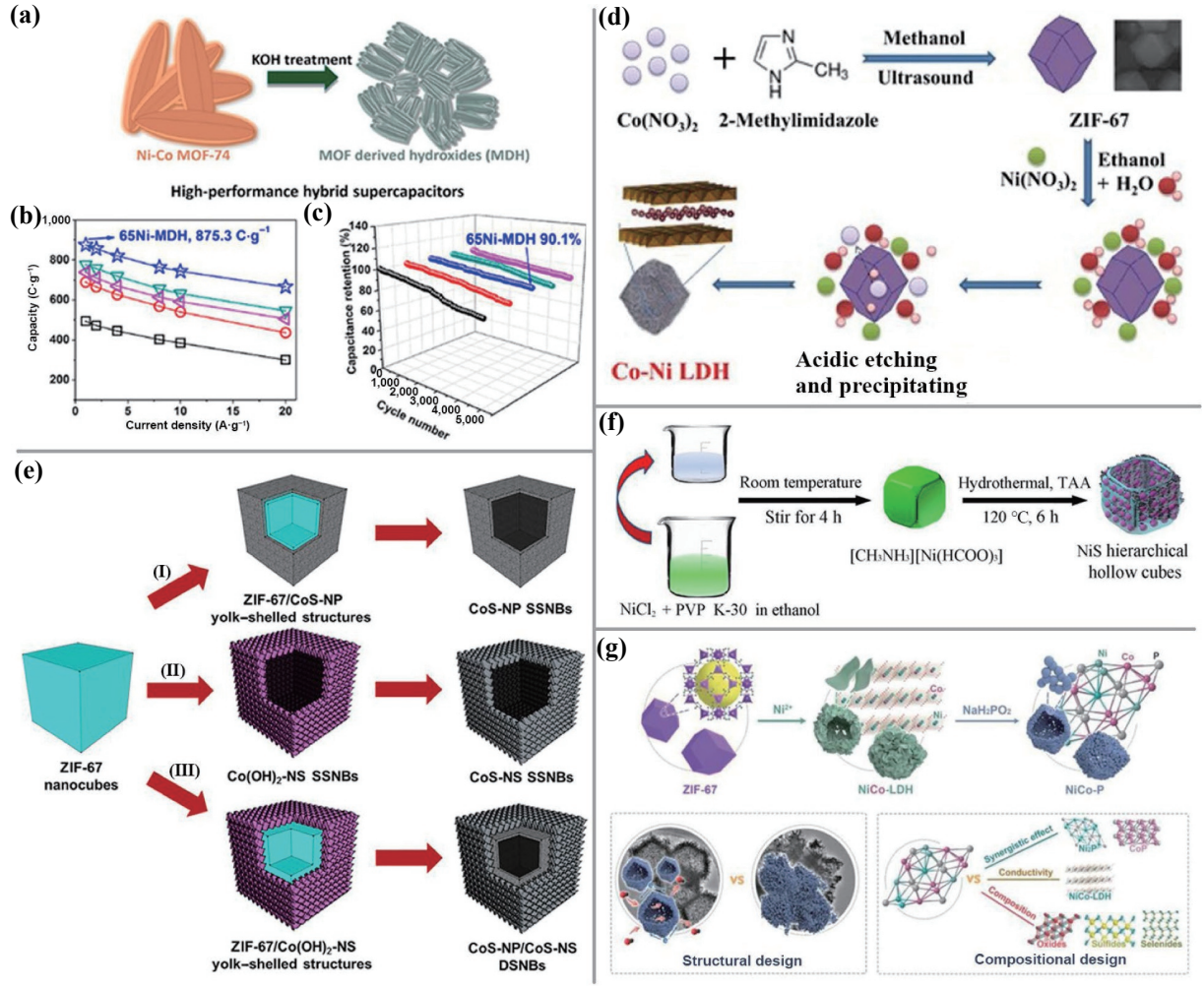

Figure 13 MOF derived metallic compounds for supercapacitors. (a) Synthetic diagram of Ni-Co MDH from MOF-74. (b) Specific capacity and (c) cycling performance of MDH electrodes with different initial Ni(II) to Co(II) ratios. Reprinted with permission from Ref. [90], © American Chemical Society 2017. (d) Schematic illustration of the synthesis procedure for Ni-Co LDH. Reprinted with permission from Ref. [91], © Springer Science+Business Media New York 2017. (e) Synthesis Procedure for Various CoS Hollow Structures. Reprinted with permission from Ref. [92], © Elsevier Inc. 2016. (f) Schematic illustration of the fabrication processes of NiS hierarchical hollow cubes. Reprinted with permission from Ref. [93], © Elsevier B.V. 2017. (g) Schematic illustration of the synthetic process of NiCo-P and the structural and compositional design of NiCo-P that boost the electrochemical performance for fast energy storage. Reprinted with permission from Ref. [94], © Liang, Z. B. et al. 2019.

derivatives as supercapacitor electrode materials. Firstly, the intrinsic activity and conductivity are determined by the properties of the components. Secondly, changing the morphology/structure of the material can expose more active sites. Thirdly, a good structure can prevent the agglomeration of the electrode materials and promote mass transfer, thus enabling excellent electrochemical properties. Considering these points, more efforts should be made to explore MOF-derived materials for highly efficient supercapacitor performance.

4 MOFs for electrocatalysis ORR

Efficient MOF-based materials provide a new platform to accelerate the sluggish ORR in fuel cells and metal-air battery cathodes due to their tunable compositions and diverse structures.

4.1 Mechanism for ORR

ORR is the key reaction occurring on the cathode of fuel cells and follows mainly two pathways: a four-electron pathway converting O_2 to H_2O directly (Eq. (1)) and a two-electron reduction pathway converting O_2 to H_2O_2 (Eq. (2)). The generated H_2O_2 may be further reduced to H_2O involving 2 electrons on another site (Eq. (3)), which is considered as sequential pathway.

$$O_2 + 4H^+ + 4e^- \rightarrow 2H_2O \quad (1)$$

$$O_2 + 2H^+ + 2e^- \rightarrow H_2O_2 \quad (2)$$

$$H_2O_2 + 2H^+ + 2e^- \rightarrow 2H_2O \quad (3)$$

Generally, the ORR reaction prefers the four-electron pathway since the two-electron pathway leads to the formation of intermediate species of H_2O_2, resulting in reduced catalytic activity. Take acidic electrolytes as an example, the possible mechanism of the ORR process on the active sites usually follows the associative pathway. O_2 is first adsorbed on the active sites, followed by protonation to form OOH*, and the reaction continues with the cleavage of the O–O bond to form O* and H_2O. H_2O is desorbed and O* takes place protonation reaction to form another H_2O. The reaction steps are as follows, where the * represents various active sites for absorbing oxygen molecules, oxygen intermediates, and final products.

$$O_2 + * \rightarrow O_2*$$

$$O_2* + H^+ + e^- \rightarrow OOH*$$

$$OOH* + H^+ + e^- \rightarrow O* + H_2O$$

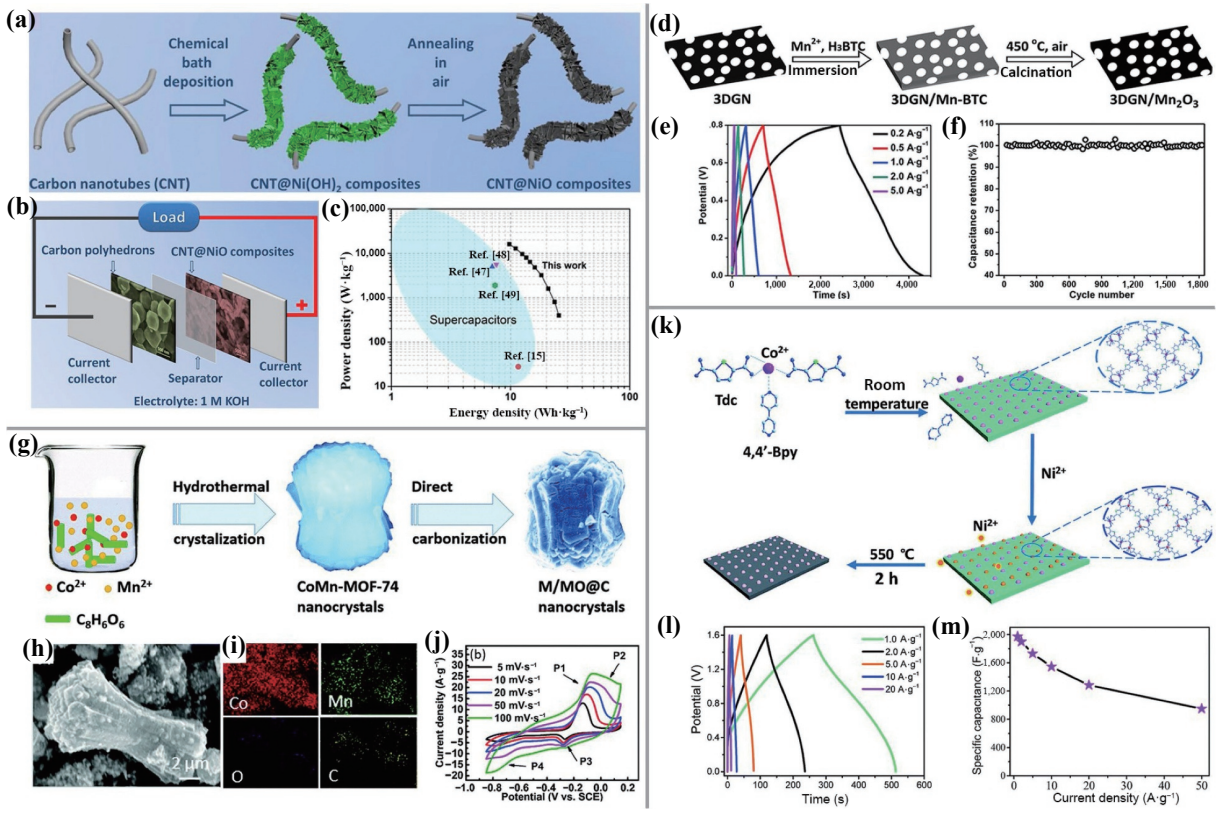

Figure 14 MOF derived metallic compound/carbon hybrids for supercapacitors. (a) Schematic illustration of the preparation of CNT@NiO composites. (b) Schematic illustration of the assembled structure of the CNT@NiO//PCPs ASC. (c) Ragone plot of the CNT@NiO//PCPs ASC. Reprinted with permission from Ref. [98], © Elsevier B.V. 2015. (d) Schematic illustration for the fabrication of 3DGN/Mn_2O_3. (e) GCD profiles of the electrodes of Mn-BTC, Mn_2O_3, 3DGN/Mn-BTC, and 3DGN/Mn_2O_3 at 0.2 A·g^{-1}. (f) Cycling performance of 3DGN/Mn_2O_3 during 1,800 charge–discharge cycles at 1 A·g^{-1}. Reprinted with permission from Ref. [99], © The Royal Society of Chemistry 2016. (g) Schematic illustration for the preparation of M/MO@C. (h) SEM images and (i) energy dispersive X-ray spectroscopy (EDS) mappings of the M/MO@C. (j) CV curves of M/MO@C-700 at various scanning rates. Reprinted with permission from Ref. [100], © The Royal Society of Chemistry 2016. (k) Schematic of the fabrication of the 2D CoNi@SNC composites. (l) Galvanostatic charge–discharge curves at different current densities of 1–20 A·g^{-1}. (m) Specific capacitance values at various current densities. Reprinted with permission from Ref. [101], © The Royal Society of Chemistry 2017.

$$O^* + H^+ + e^- \rightarrow OH^*$$

$$OH^* + H^+ + e^- \rightarrow H_2O$$

Although tremendous efforts have been made to find the rate-determining step for ORR, there is no clear conclusion because the reaction pathway depends to a large extent on the catalyst and environmental parameters, such as temperature, solvent, and electrode potential. In most cases, the total ORR rate is determined by one of these three steps: 1) first electron transfer to the adsorbed O_2 molecule, (2) O_2 hydration, and (3) final desorption of H_2O (Fig. 15). Over the past few decades, extensive research efforts have been devoted to the development of non-precious metal catalysts [104–107]. In recent years, MOF-based materials as ORR electrocatalysts have been widely studied due to their ability to design and regulate chemical composition at the molecular level, and their highly porous frameworks can accelerate mass and charge transfer.

4.2 Pristine MOFs for ORR

Pristine MOFs can be used as ORR electrocatalysts directly because their abundant pores facilitate the transport of O_2 and water, and their abundant active metal sites accelerate the electrochemical process. Transition metal porphyrin complexes, especially Fe(III) porphyrin complexes related to hemoglobin structure, have strong interaction with O_2. Hence, several MOFs containing Fe(III) porphyrins have been reported. A Zr-based porphyrin MOF (PCN-223), containing a large triangular channel with a partial arrangement of Fe(III) porphyrins, exhibited

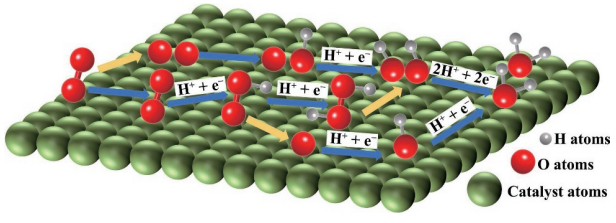

Figure 15 Illustration of the reaction pathway of ORR.

outstanding performance in acidic environments (Figs. 16(a) and 16(b)) [108]. The strong interaction between the porphyrin linker and Zr_6-oxygen cluster and the redox inertia of Zr^{4+} ions contribute to the structural stability during the redox cycle. As shown in Figs. 16(c) and 16(d), Dinca. et al. [109] introduced $Ni_3(HITP)_2$ as an intrinsically conductive MOF that functioned as a well-defined, tunable oxygen reduction electrocatalyst in an alkaline solution. Zhang et al. reported a nanocaged copper-based MOF (NPC-4) containing copper active sites [110] (Figs. 16(e) and 16(f)). The nanocages with a diameter of about 0.6 nm are sufficient for gas molecules to pass through, but the pores are occupied by solvent N,N-dimethylacetamide (DMA) molecules in the synthesized MOF. Without activation, the electrochemical performance of the electrode mainly depends on the electron transfer between the electrode surface and some metal ions. Activated by solvent exchange methods, the space inside the nanocages can be released, exposing a large number of open metal sites. By removing the solvent molecules in the nanocage, dissolved oxygen enters the nanocage and is reduced by Cu^+.

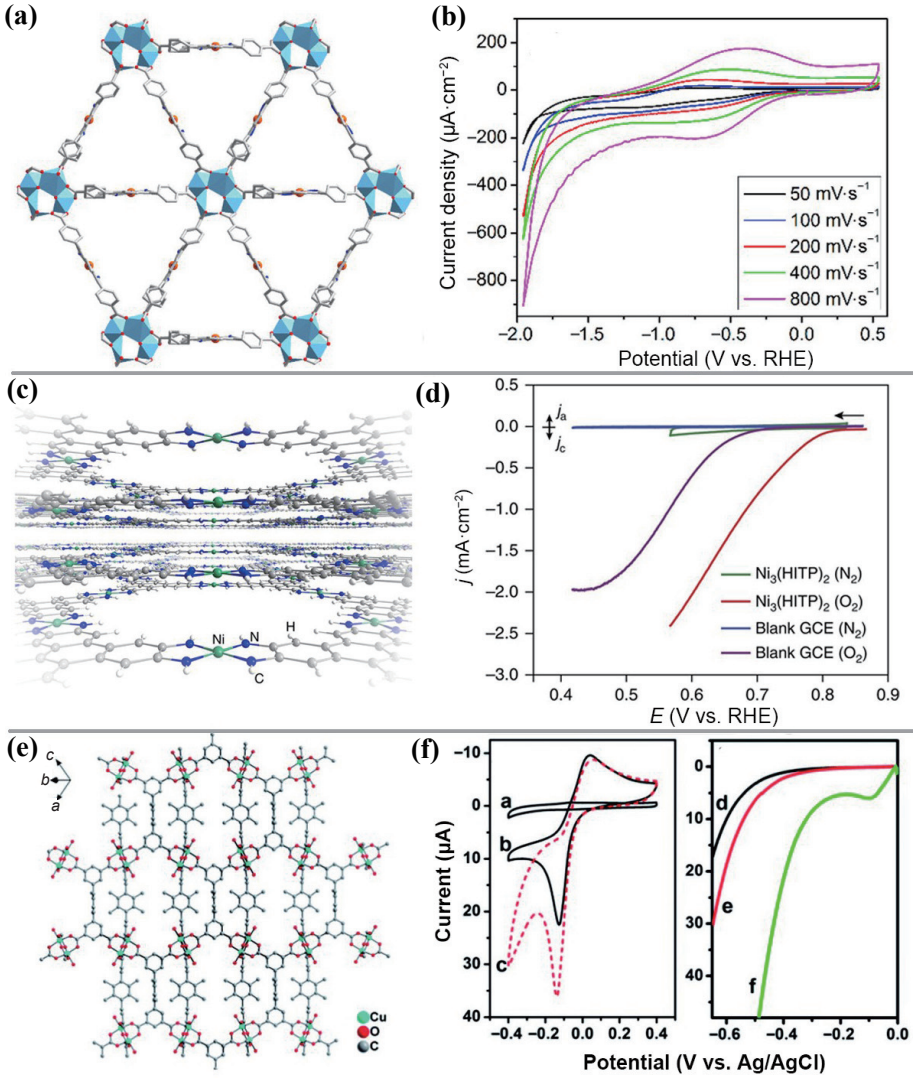

Figure 16 Pristine MOFs for ORR. (a) Crystal structure of PCN-223-Fe MOF. (b) Variable scan rate cyclic voltammograms of PCN-223-Fe films measured. Reprinted with permission from Ref. [108], © American Chemical Society 2017. (c) The framework structure of Co-Al-PMOF. (d) Linear sweep voltammetry (LSV) curves for different samples in O_2-saturated 0.1 M H_2SO_4. Reprinted with permission from Ref. [109], © Miner, E. M. et al. 2016. (e) Crystal structure of NPC-4. (f) CV and LSV curves. Reprinted with permission from Ref. [110], © The Royal Society of Chemistry 2014.

4.3 MOF composites for ORR

To date, many MOFs and functional materials have been successfully self-assembled to obtain composite materials, which can be divided into two categories according to the distribution of the main active sites. The first category is the combination of MOFs and conductive carbon materials (carbon nanotubes, graphene, heteroatom doped carbon, etc.), in which MOFs are the main active species in ORR reaction, while carbon materials provide a conductive network. For instance, Sohrabi et al. [111] reported a PCN-222-G-py composite via the connection of pyridine-functionalized graphene nanosheets (G-py) to the iron centers of porphyrin struts located in MOF (PCN-222(Fe)) (Fig. 17(a)). Pyridine functional groups act as axial ligands to change the geometry and electronic structure of graphene centers and promote electron transfer from graphene centers to iron centers. PCN-222-G-py showed excellent ORR performance and acceptable durability in acidic medium cycles. Compared with commercial Pt/C, the ORR potential peak of the composite had a positive shift of about 282 mV. Jahan et al. [112] reported a hybrid of pyridine-functionalized graphene with iron–porphyrin MOF composite for ORR (Fig. 17(b)). Our group developed a simple method for the preparation of highly efficient ORR catalysts based on covalent organic polymer (COP) synthesized in sit-in the nanoconfined space of highly ordered MOF (Fig. 17(c)) [113]. After a series of characterization, the MOF template ensured that the electrocatalyst had a high specific surface area and uniformly distributed small metal/nitrogen active sites, leading to highly efficient ORR electrocatalytic activity. Feng et al. [114] reported a PcCu-O_8-Co 2D MOF material mixed with two-dimensional conjugated MOF with carbon nanotubes, which exhibited well electrocatalytic ORR performances (Figs. 17(d)–17(f)).

The second type is the combination of MOFs with metals or metal compounds, in which metals or metal compounds are active species and MOFs act as supports or reaction chambers. He et al. [115] reported a bifunctional electrocatalyst based on MIL-101(Cr) with various surface Co^{III} and Co^{II} contents via an oxidation or reduction treatment during an impregnation process (Fig. 17(g)). The catalytic activities of the electrocatalysts toward the ORR in an alkaline electrolyte were tested using a rotating disk electrode technique. The results exhibited Co/MIL-101(Cr)-R had a higher surface Co^{II} content and promoted higher ORR responses.

4.4 MOF derivatives for ORR

Compared with the attempts to use pure MOFs and MOF composites for ORR, more efforts have been made to convert them into inorganic functional materials with composition,

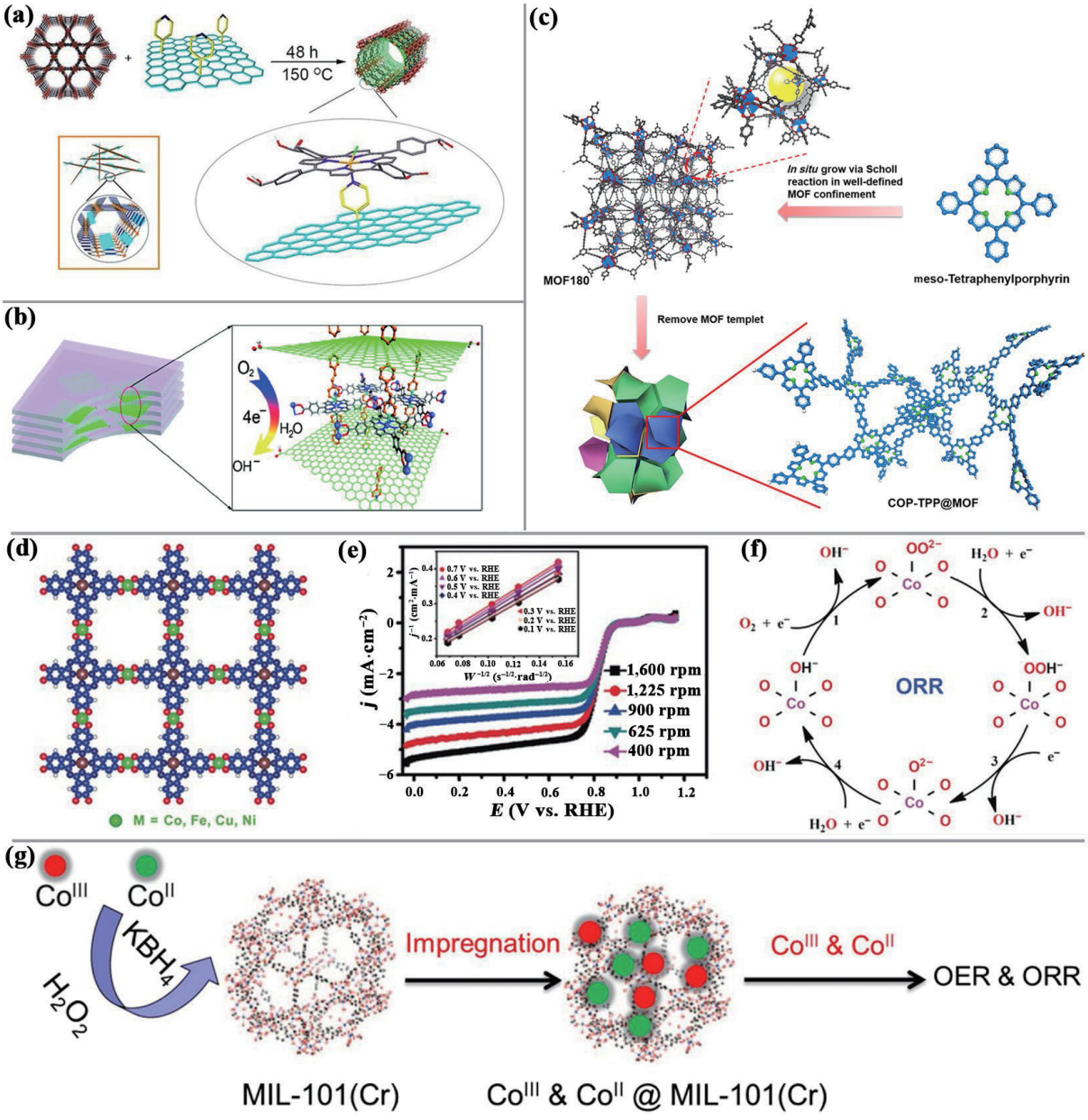

Figure 17 MOF composites for ORR. (a) Schematic illustration of the preparation of PCN-222-G-py. Reprinted with permission from Ref. [111], © Wiley-VCH Verlag GmbH & Co. KGaA, Weinheim 2016. (b) $(G\text{-dye-FeP})_n$ MOF formed via reaction between $(Fe–P)_n$ MOF and G-dye. Reprinted with permission from Ref. [112], © American Chemical Society 2012. (c) Schematic illustration of nanoconfinement-induced synthesis of COP-TPP@MOF catalyst. Reprinted with permission from Ref. [113], © American Chemical Society 2017. (d) Schematic structure of PcCu-O_8-M. (e) ORR polarization curves. (f) Proposed reaction mechanism. Reprinted with permission from Ref. [114], © WILEY-VCH 2019. (g) The illustration of the design and preparation of the bifunctional electrocatalyst. Reprinted with permission from Ref. [115], © Hydrogen Energy Publications, LLC 2015.

morphology, and controllable size [116]. Compared with traditional porous materials, MOF derived materials have some unique advantages. For example, MOFs derived materials can effectively retain the structure, morphology, and size of original MOFs. There are many kinds of MOFs and a variety of derived materials can be prepared [117–119]. According to their chemical composition, these derivatives are classified into the following three categories, and their recent progress as ORR electrocatalysts is summarized.

4.4.1 *Metal-free carbon materials for ORR*

In general, MOF-derived metal-free carbon materials are usually obtained by high-temperature pyrolysis and etching with acids such as HCl, HF, and HNO_3. Additionally, some metals with low boiling points will evaporate in the form of steam during high-temperature calcination. For example, the Zn^{2+} in classic materials of ZIF-8 will evaporate at around 900 and leave many pores. It was found that nitrogen-doped carbon substrates such as hollow carbon spheres, graphene oxide, and carbon nanotubes all exhibit excellent ORR properties because N can provide lone pair electrons to form Π-graphene carbon. Wang et al. [120] prepared a novel defect-rich 3D nanosheet bonded polyhedral carbon by pyrolysis of metal organic frameworks sealed with NaCl (Figs. 18(a) and 18(b)). The results showed that NaCl crystal can not only be used as pore-forming agent to help form defect-rich structure with high porosity, but also can be used as a sealed reactor to effectively preserve the decomposed intermediate species and promote nitrogen doping in the carbon network during pyrolysis. Due to the high content of N doping, abundant defects, and good interface contact between PC and carbon nanosheets, the catalyst had a good electrocatalytic activity for ORR, excellent stability, well tolerance to methanol, and a four-electron reaction path. Chai et al. [121] successfully prepared N-doped carbon spheres; compared with commercial Pt/C, it

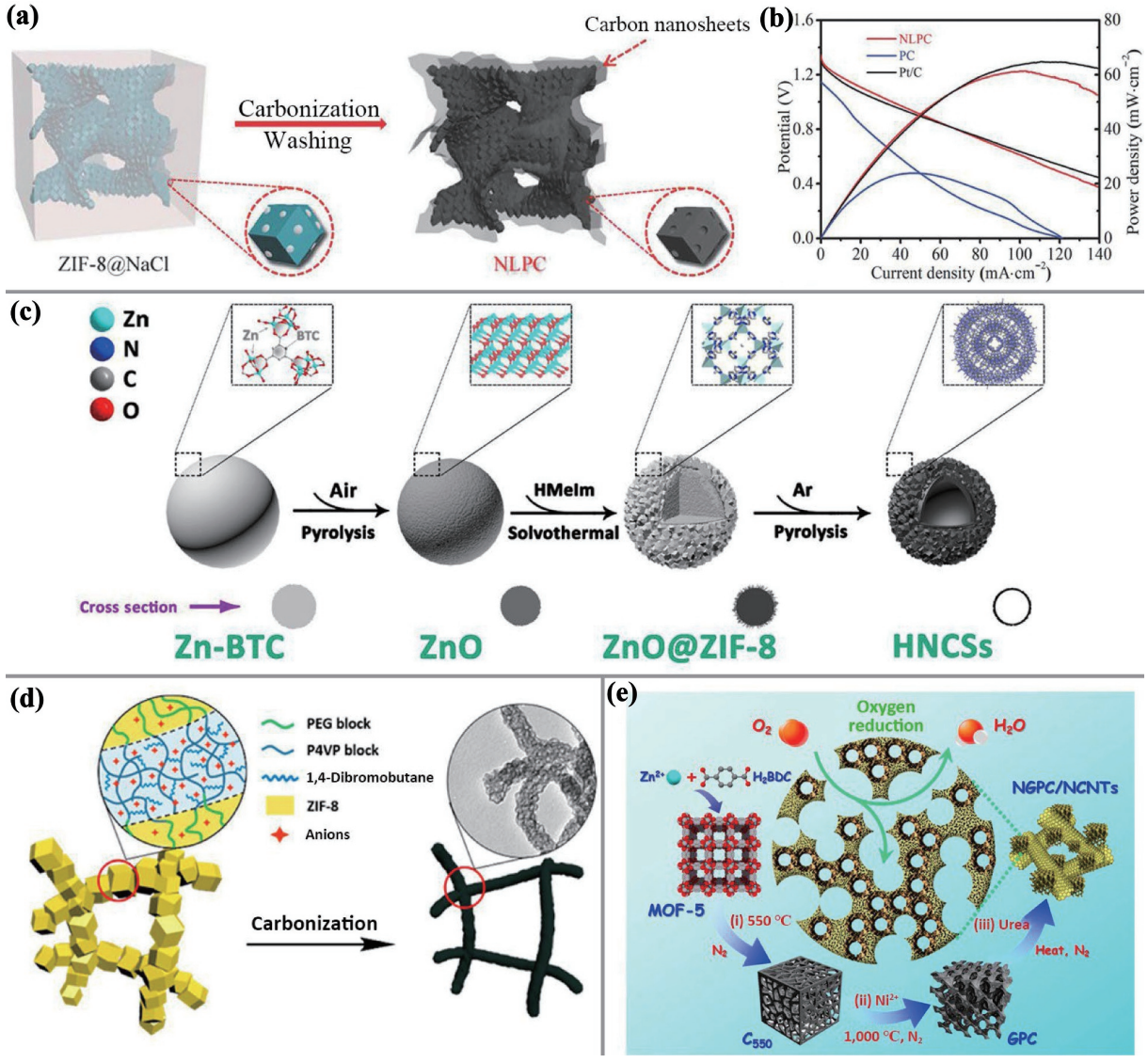

Figure 18 MOF derived metal-free carbon materials for ORR. (a) Schematic illustration of the synthesis of defect-rich nanosheet linked polyhedron carbon. (b) Polarization and power density curves. Reprinted with permission from Ref. [120], © WILEY-VCH Verlag GmbH & Co. KGaA, Weinheim 2018. (c) Schematic preparation of hollow N-doped carbon spheres. Reprinted with permission from Ref. [121], © Elsevier Ltd. 2019. (d) Illustration of the synthesis of multiheteroatom-doped porous carbon nanofibrous network. Reprinted with permission from Ref. [123], © American Chemical Society 2017. (e) Schematic illustration of the stepwise structural evolution from MOF-5 to NGPC/NCNTs. Reprinted with permission from Ref. [122], © American Chemical Society 2015.

exhibited relatively high electrocatalytic ORR activity, excellent reaction selectivity, well cycle stability, and long-term methanol durability (Fig. 18(c)). Together with the other two reported carbonaceous ORR catalysts, including solid carbon spheres (SCSs) and nitrogen-doped graphitic porous carbons (NGPCs), the hollow nitrogen-doped carbon spheres (HNCSs) possessed the lowest Tafel slope of 65.7 mV·dec^{-1} which is close to Pt/C (62.6 mV·dec^{-1}), and showed much enhanced ORR activity (J_L = 5.34 mA·cm^{-2}) and stability (retention = 96.5%, time = 10 h). Hong et al. [122] developed an effective method to synthesize highly graphitized NGPC/NCNT hybrids from MOF-5 through continuous carbonization, catalytic graphitization, and nitriding processes (Fig. 18(e)). The NGPCs/NCNTs had unique heterostructures to form interlinked three-dimensional conductive networks by bridging dissociated NGPCs with NCNTs, which showed superior ORR activities.

Combined with the synergistic effect between different dopants and high porous structure, MOF-derived multi-element doped porous carbon materials are expected to further improve the catalytic activity of ORR. Remarkably, controllable multi-heteroatoms (S, N, B, and P) doped porous carbons were synthesized by Huang et al. [123] using a 3D network constructed by ZIF-8 coated wormlike micelles as a template (Fig. 18(d)). The uniform and highly pure wormlike micelles developed are essential because they are not only responsible for the formation of hierarchical porous structure, but also serve as a multifunctional platform for heteroatom doping. The doping of S, N, B, P, and other heteroatoms makes the prepared porous carbon have good oxygen reduction reaction performance, which is comparable to the commercial 20% Pt/C.

4.4.2 *Carbon-based material containing precious metals for ORR*

The precious metals Pt and Pd have been recognized as the most advanced ORR electrocatalysts. Through the reasonable combination of noble metal-containing materials and MOFs, the ORR electrocatalyst with high utilization and strong interaction with carbon support can be obtained [124]. Zou et al. [125] reported the formation of PtNi nanoparticles with an average diameter of about 10 nm embedded in a few carbon layers (PtNi@C) and their ORR performance (Figs. 19(a)–19(d)). The 2-methylimidazole-Pt-Ni composite (MPN) with similar MOF structure was synthesized by solvothermal method and then

calcined at high temperature. Wang et al. [126] developed a new approach to prepare Pt_3Co intermetallic nanoparticles for ORR electrocatalysis (Figs. 19(e)–19(g)). The atom-dispersed Co sites were initially embedded in MOF derived carbon and formed an ordered Pt_3Co structure with Pt nanocrystals. The results showed that the activity and stability of the optimized Pt_3Co nanoparticle catalyst were significantly improved; the half-wave potential was as high as 0.92 V and only 12 mV was lost when the potential was 30,000 cycles between 0.6–1.0 V. The atomic-scale element mapping showed that the structure of the intermetallic compounds remained highly ordered after the accelerated stress test. Additionally, Wang et al. [127] proposed collaborative nanostructure design strategy based on platinum nanoparticles (Pt NPs) and ultra-thin two-dimensional MOFs for bifunctional electrochemical catalysts. The PtNPs@MOFs composites have achieved significant improvement in the activity and durability of ORR (Figs. 19(h) and 19(i)). Chen et al. [128] designed and fabricated a novel mutual-interacted Pt-CeO_2-C ternary nanostructure from a Ce-based metal organic framework (Ce-MOF). In this unique nanostructure, by calcination, a large number of tiny CeO_2 nanoclusters (~ 2 nm) can be produced by calcination of Ce-MOF itself, which are uniformly embedded in the MOF-derived porous carbon matrix (Figs. 19(j)–19(l)). Meanwhile, the deposited Pt nanoclusters without surfactant had good contact with carbon nanoclusters and CeO_2 nanoclusters. Yu et al. [129] reported a general method for the synthesis of Pd@PdO-Co_3O_4 nano cubes using zeolite-type MOF as a template. The synthesized materials have high electrocatalytic activity for oxygen evolution reaction (OER) and ORR, which is comparable to RuO_2 and Pt/C electrocatalysts on the market, but their cycling performance and stability are much higher than those of RuO_2 and Pt/C electrocatalysts.

4.4.3 Carbon-based material containing non-precious metals for ORR

In view of the great diversity of MOFs, novel carbon-based materials with controllable size, shape, and composition can be prepared after high-temperature pyrolysis by selecting MOF precursors with different organic ligands and metal atom compositions. MOFs-derived carbons have promising applications in ORR due to their high electrical conductivity, rich and diverse pore structures, and tunable elemental compositions.

4.4.3.1 Atomically dispersed metal sites

In recent years, MOFs-derived atomic dispersive metal sites (ADMS) electrocatalysts have emerged rapidly (Fig. 20) [130, 131]. Briefly, a single atomic electrocatalyst can be defined as a catalyst with atom-dispersed active metal atoms on the support. These materials have the advantages of uniform dispersion of active sites, high selectivity, high atom utilization efficiency, and strong interaction between active sites and supports, which can improve the catalytic performance [132–134].

Using MOFs or external precursors as Fe sources, Fe-N_x-C structure ORR electrocatalysts derived from MOFs have been extensively studied and have shown high catalytic performance. Li et al. [135] prepared a highly active and stable monatomic Fe/N doped porous carbon (ISA Fe/CN) catalyst with Fe loading rate up to 2.16 wt.% (Figs. 21(a)–21(c)). The catalyst had excellent ORR performance and a half-wave potential ($E_{1/2}$) of 0.900 V, which is

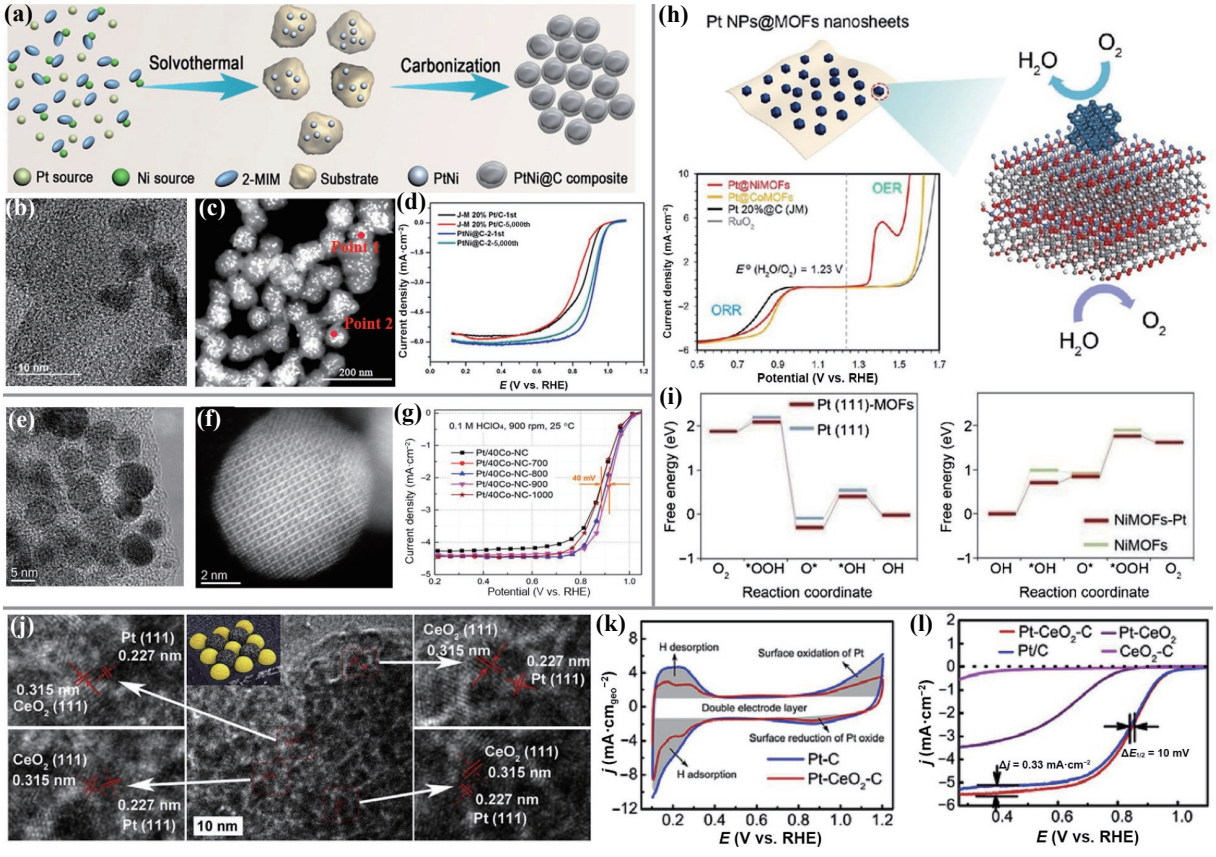

Figure 19 MOF derived carbon-based material containing precious metals for ORR. (a) Schematic illustration of the preparation of PtNi@C composites. (b) High-resolution TEM (HRTEM) and (c) high-angle annular dark-field (HAADF) images. (d) LSV curves for Pt/C and PtNi@C-2 samples after the 1st and 5,000th cycles. Reprinted with permission from Ref. [125], © American Chemical Society 2019. (e) HRTEM images of Pt/40Co-NC-900 catalyst. (f) Atomic resolution HAADF-STEM image of Pt_3Co nanoparticle. (g) LSV curves at different temperatures. Reprinted with permission from Ref. [126], © American Chemical Society 2018. (h) ORR performance diagram. (i) Free energy diagrams for ORR. Reprinted with permission from Ref. [127], © Elsevier B.V. 2019. (j) HRTEM images of Pt-CeO_2-C. (k) CV curves of Pt-CeO_2-C and Pt-C in N_2-saturated 0.1 M $HClO_4$ solution. (l) LSV curves. Reprinted with permission from Ref. [128], © Elsevier Ltd. 2018.

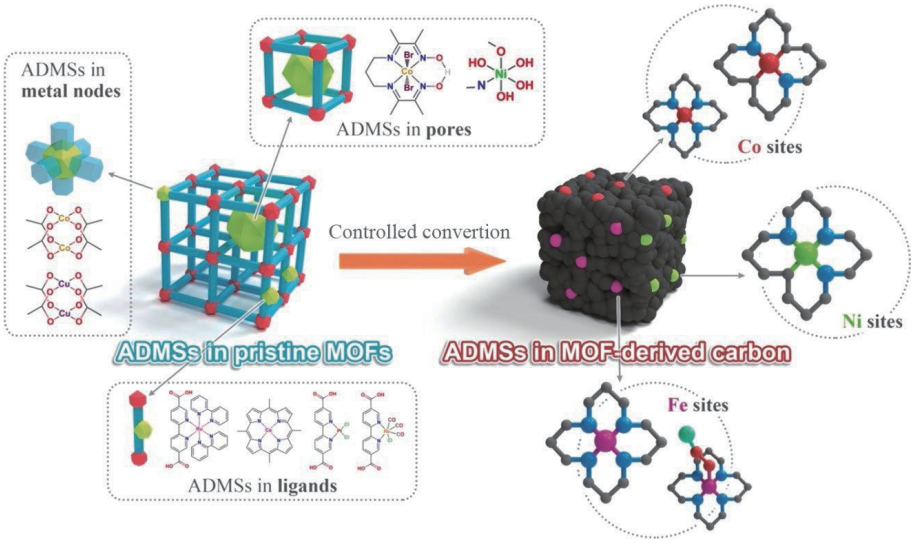

Figure 20 Schematic illustration of different types of ADMSs in MOF-derived carbon. Reprinted with permission from Ref. [130], © Wiley-VCH Verlag GmbH & Co. KGaA, Weinheim 2018.

better than the reported commercial Pt/C catalysts and most non-noble metal catalysts. In addition to the extremely high dynamic current density (J_K) of 37.83 mV·cm^{-2} at 0.85 V, it also had well methanol tolerance and excellent stability. Experiments showed that keeping Fe as an isolated atom and adding nitrogen are necessary conditions to provide high performance. Wu et al. [136] developed a monatomic Fe catalyst without metal agglomeration by chemically doping Fe ions into a ZIF network and then performing a one-step thermal activation (Figs. 21(d)–21(f)). The chemical doping process is the key to the formation of possible Fe-N_4 complexes connected to three-dimensional organic skeleton nanocrystals. Subsequent thermal activation transformed these to ORR-active atom FeN_4 sites embedded in the porous carbon phase. The new atomic Fe catalyst achieved excellent ORR activity in acidic electrolytes along with significantly enhanced stability. Zhao et al. [137] synthesized Co-N-C catalysts via pyrolysis of Zn/Co-ZIF precursor, and this type of carbon nano hybrid material had a hierarchical pore structure and high specific surface area (Figs. 21(g)–21(i)). The Co-N-C catalyst had higher ORR activity ($E_{1/2}$ = 0.9 V), which is comparable to 20 wt.% Pt/C ($E_{1/2}$ = 0.835 V) in an alkaline medium. Wu et al. [138] reported an effective strategy for the synthesis of atom dispersed Mn-N-C catalysts from environmentally friendly aqueous solutions instead of conventional organic solvents (Figs. 21(j)–21(l)). This innovative synthesis method produced an extremely high surface area to accommodate the increased density of MnN_4 active sites, which has been verified by X-ray absorption spectroscopy and advanced electron microscopy. The obtained Mn-N-C catalyst exhibited good ORR activity and significantly enhanced stability, with a peak power density of 0.39 W·cm^{-2} at 1.0 bar H_2-air condition, which is better than most PGM-free ORR catalysts. With the further study of isolated-atomic dispersion catalysts, bimetallic and even polymetallic catalysts (e.g., Fe-Co, Fe-Ni, Mn-Co, and Fe-Zn) have also been widely investigated. For instance, Li et al. [139] developed a host–guest strategy to construct a Fe-Co dual sites electrocatalyst embedded on N-doped porous carbon and demonstrated its activity for oxygen reduction in acidic electrolytes (Figs. 21(m)–21(o)). Fuel cell experiments showed that the performance of (Fe, Co)/N-C catalyst in H_2/O_2 and H_2/air was better than that of most Pt-free catalysts reported.

4.4.3.2 Metal-based nanoparticles

Moreover, a variety of metal compounds (oxides, carbides, sulfides, etc.) combined with carbon composites can also be obtained through pyrolysis of MOFs. Lou et al. [140] used a bimetallic organic framework as a precursor to construct abundant MnO/Co heterointerfaces in porous graphite carbon (MnO/Co/PGC) polyhedra through a simple hydrothermal calcination route. *In situ* generated cobalt nanocrystals not only produced well-defined heterogeneous interfaces with high electrical conductivity, overcoming poor ORR activity, but also promoted the formation of graphite carbon. Li et al. [141] reported the preparation of cobalt-based nanoparticles embedded in hollow nitrogen-doped polyhedron by a two-step pyrolysis-oxidation method using Co based MOF (ZIF-67) as the precursor (Fig. 22(a)). Moreover, a composite material constructed from iron carbide nanocrystalline-embedded carbon nanotubes encapsulated in a porous carbon matrix was successfully prepared, which exhibited remarkable ORR performance in 1 M KOH electrolyte (Figs. 22(b)–22(d)) [142].

5 Conclusion and outlook

This review provides an overview of the recent development of MOF-based materials as highly electrode materials for supercapacitors and electrocatalysis ORR in fuel cells. In the last few decades, coordination chemistry has made a significant influence. It is also true for the fast-growing field of supercapacitors and electrocatalysis ORR based on various MOF electrode materials. As mentioned above, MOF-based materials offer great opportunities for the fabrication of capacitive and battery-type electrodes for supercapacitors and electrocatalysis ORR possessing desired energy/power density meanwhile. But there is still a large room for improvement. Many of the challenges in this field must be addressed if significant improvements are to be made:

(a) MOFs can be directly used as the electrode materials in supercapacitors and electrocatalysis ORR. Their unique advantages, including high porosity, high surface area, adjustable pore size, and controllable structure make great contributions to electrochemical performance. However, the stability of MOFs in electrolytes needs to be improved under operating potential. Also, most traditional MOFs have poor electrical conductivity due to the presence of organic ligands, and thus have the inferior capacity and cycling stability.

(b) MOF composites were developed to compensate for the shortcomings of MOFs, which can effectively combine the advantages of MOF with a variety of functional materials.

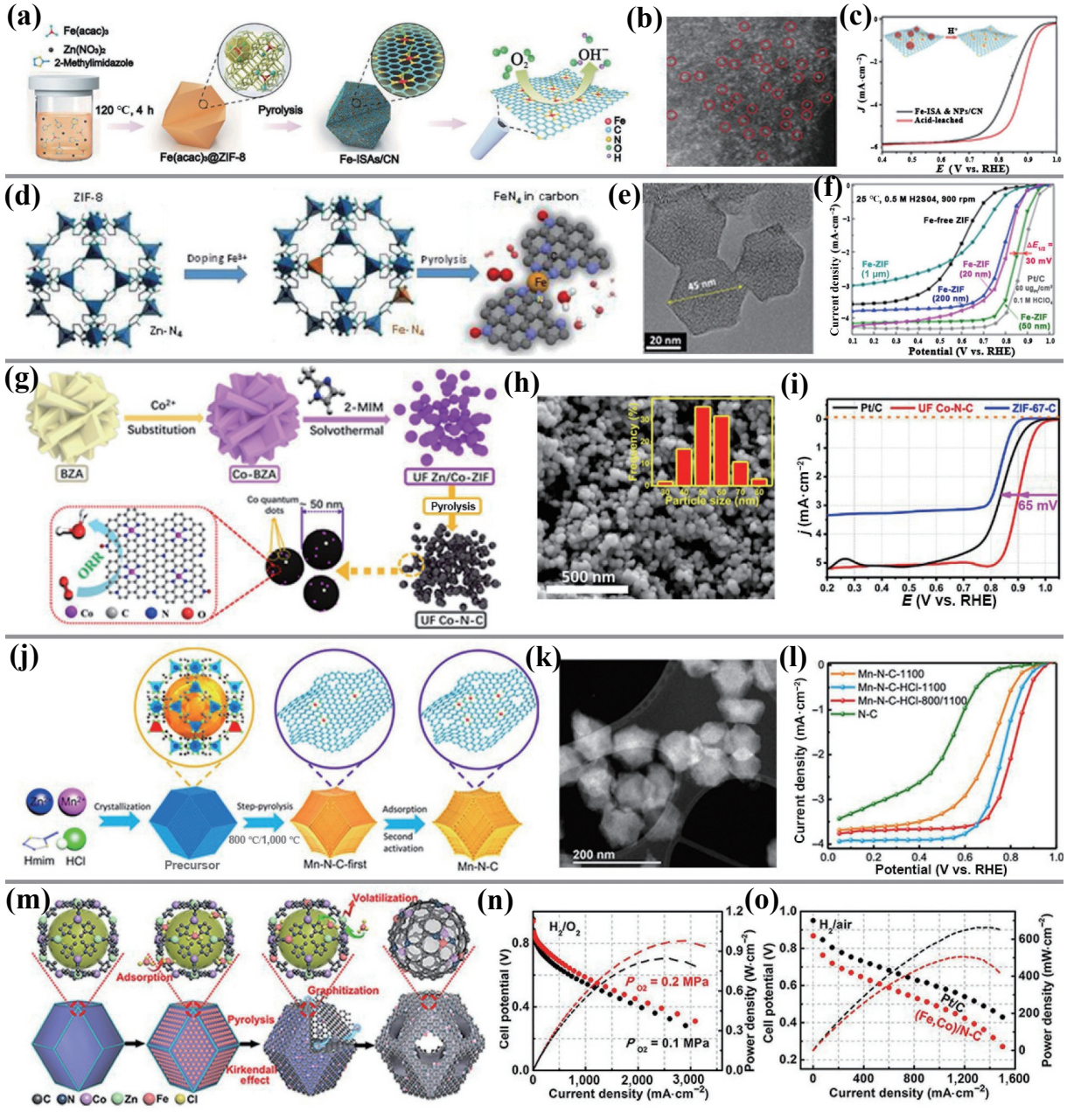

Figure 21 MOF-derived carbon materials with atomically dispersed non-precious metal sites for ORR. (a) Schematic illustration of the formation of Fe-ISAs/CN. (b) Enlarged images of the Fe-ISAs/CN. (c) ORR polarization curves. Reprinted with permission from Ref. [135], © Wiley-VCH Verlag GmbH & Co. KGaA, Weinheim 2017. (d) Synthesis principles of Fe-doped ZIF-derived catalysts. (e) TEM images. (f) ORR polarization plots for Fe-ZIF-derived catalysts and Pt/C catalysts at 900 rpm. Reprinted with permission from Ref. [136], © American Chemical Society 2017. (g) Schematic illustration of the synthetic procedure of UF Co-N-C. (h) SEM image of UF Co-N-C. (i) Electrocatalytic ORR performance. Reprinted with permission from Ref. [137], © American Chemical Society 2020. (j) Aqueous synthesis scheme for Mn-N-C catalysts. (k) STEM images. (l) ORR polarization curves. Reprinted with permission from Ref. [138], © American Chemical Society 2020. (m) Preparation of (Fe,Co)/N-C. (n) H_2/O_2 fuel cell polarization plots. (o) H_2/air fuel cell polarization plots. Reprinted with permission from Ref. [139], © American Chemical Society 2017.

Although MOF composites have made great contributions to electrochemical applications, many defects still need to be overcome. In the synthesis of MOF composite materials, the precise control of complex size and position is particularly difficult. Most synthetic methods have inherent limitations, which require sensitive and expensive organic solvents, and usually require multiple steps. Hence, the combination of various materials and even composite materials with other MOFs is worth further research.

(c) For carbonaceous materials acquired from MOFs and used as electrode materials, their capacitance and electrocatalytic capacity are not enough to achieve high energy density. The construction of MOF derived carbon with reasonable porous properties (including high specific surface area and porosity), good pore structure, and appropriate composition may be an effective strategy to improve electrochemical performance. To further improve the performance of derived porous carbon, the doping of heteroatoms such as N, S, and P is an effective method, which can be realized not only in the preparation of MOFs, but also in the post-processing stage. However, controlling the proportion of these species and the ratio of heteroatoms remains a major challenge.

(d) For MOF derived metallic compounds, the current research mainly focuses on the preparation of metal oxides, hydroxides, sulfides, phosphides, and other nanostructures materials. In addition, metallic compound composites are also of great concern due to their wide applications and can be obtained from MOFs by simple methods. For the resulting metal compounds, the electrical

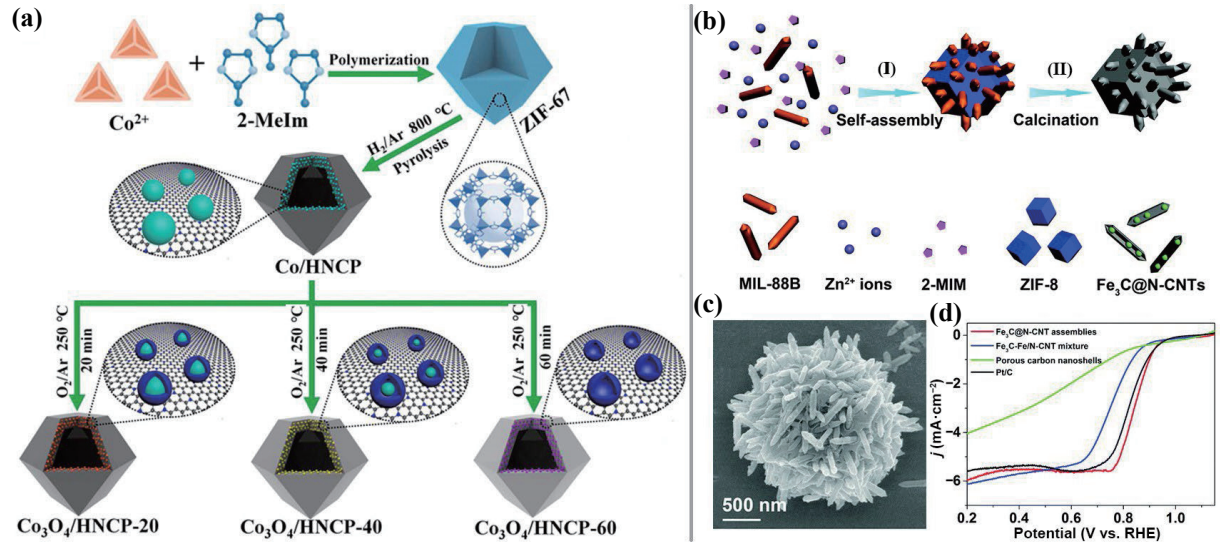

Figure 22 MOF-derived carbon materials with metal-based nanoparticles for ORR. (a) Illustration of fabrication of a series of Co-Co_3O_4-based nanoarchitectures embedded in hollow nitrogen-doped carbon polyhedra. Reprinted with permission from Ref. [141], © American Chemical Society 2018. (b) Schematic illustration of the formation process of Fe_3C@N-CNT assembly. (c) FESEM image. (d) LSV curves. Reprinted with permission from Ref. [142], © The Royal Society of Chemistry 2016.

conductivity needs to be improved to ensure a high energy/power density. Additionally, since these metallic compounds usually undergo redox reactions in the electrochemical reaction, their cyclic stability is often not very ideal. The growth of MOF derived metal compounds onto the free-standing conductive substrate is an effective method to obtain ideal electrode materials.

In conclusion, MOFs and their derived nanomaterials show great potential in the field of supercapacitors and electrocatalytic ORR systems due to their unique properties. However, there are still some problems and room for improvement in the synthesis and pyrolysis of MOFs. On the one hand, it is a great challenge to purposefully prepare high conductivity MOFs and directly apply them to energy storage and conversion. On the other hand, the structure and controllable morphology of porous carbon or metal compound composites derived from MOFs need to be further explored, and the uniform distribution between metal matrix and carbon matrix is still not very easy to obtain. In addition, the bond effect, component proportion, and particle distribution of metal particles and carbon in MOFs derived composites need to be further studied.

To overcome the above challenges, some solutions and potential development trends might be noted as follows:

For supercapacitors, how to further improve the conductivity is very important. Most MOF materials have poor conductivity, so it is necessary to deepen the understanding of the conductivity mechanism of metal coordination materials, design and develop new conductive MOFs. On the other hand, the conductivity of MOFs is further improved by combining with highly conductive materials (carbon nanotubes, graphene oxide, activated carbon, conductive polymers, etc.). Constructing MOFs with reasonable specific surface area and porosity, abundant pore structure, and appropriate composition is an effective strategy to improve capacitance. High capacity and power density of supercapacitors are achieved by developing highly vertically oriented 2D MOFs and their composites and derivatives by making full use of their surfaces and active sites. Computer screening of how electrode materials interact with electrolytes will provide profound guidance for further development of electrode materials.

For ORR, atomically dispersed metal-nitrogen coordination structure (M-N_x) is generally believed that the active center of ORR. Along this line of thought, some porphyrins, phthalocyanine-based metal macrocycles used as the original electrocatalysts show great potential. In the process of synthesizing MOFs, heteroatoms such as fluorine, sulfur, nitrogen, and oxygen are precisely introduced, which can change the electronic structure of metal active center, thus regulating the ORR performance. Synergistic effects could be achieved by introducing bimetallic or even trimetallic atom pairs to improve catalytic activity and stability (Table 2). Additionally, besides high active sites, the utilization of active sites and efficient charge transfer are essential to achieve excellent ORR performance, so it is worth considering to construct MOFs with abundant porosity by selecting suitable organic ligands. *In situ* characterization techniques (Fourier transform infrared spectroscopy (FT-IR), Raman spectroscopy (Raman), and X-ray absorption near edge structure (XANES)) will help to understand the evolution process and reaction mechanism of electrocatalysts. With the development of quantum chemistry, the combination of experimental and theoretical research will create new opportunities for the discovery and breakthrough of advanced electrocatalysts.

Although there are still many challenges to its wide application in electrochemical reactions, we believe that this emerging field deserves more effort and attention. There is no doubt that MOFs will continue to promote the development of the electrochemical field. From a practical point of view, the abundant elements on earth should be used to prepare MOF based materials to fully address the pressing energy and environmental challenges facing our society. Through continuous research, we will have the opportunity to witness a new technological revolution in renewable energy and environmental science in the near future.

Acknowledgements

This work was supported by the National Key Research and Development Program of China (No. 2019YFA0210300), the Natural Science Foundation of China (No. 21922802), the Beijing Natural Science Foundation (No. JQ19007), Talent Cultivation and Open Project (No. OIC-201801007) of State Key Laboratory of Organic-Inorganic Composites, "Double-First-Class" Construction Projects (Nos. XK180301 and XK1804-02), and the Distinguished Scientist Program at BUCT (No. buctylkxj02).

Table 2 MOF-based materials for ORR

MOFs/composites/derivatives	Onset potential (V)	Half-wave potential (V)	Electrolyte
Cu-BTC [143]	0.93	0.82	0.1 M phosphate
$Ni_3(HITP)_2$ [109]	0.82	0.71	0.1 M KOH
FePc/rGO [112]	0.95	0.83	0.1 M KOH
PcCu-O_8-Co/CNT [114]	0.97	0.85	0.1 M KOH
CuS@Cu-BTC [144]	0.91	0.83	0.1 M KOH
N-PC [145]	0.88	0.81	0.1 M KOH
P,N-PC [146]	0.92	0.80	0.1 M KOH
Co_9S_8/NC [147]	0.92	0.82	0.1 M KOH
Co/Co_3O_4-C [148]	—	0.80	0.1 M KOH
Co-N-C [149]	1.1	0.87	0.1 M $HClO_4$
Co/N–PC [150]	0.9	0.761	0.1 M $HClO_4$
$FeCoN_x$/C [151]	1.02	0.86	0.1 M $HClO_4$
Fe,Mn/N–C [152]	1.052	0.928	0.1 M KOH
Ni-N-C [153]	1.046	0.938	0.1 M KOH
Mn-N-C [154]	0.92	0.80	0.1 M $HClO_4$

References

[1] Li, L.; Lu, F.; Xue, R.; Ma, B. L.; Li, Q.; Wu, N.; Liu, H.; Yao, W. Q.; Guo, H.; Yang, W. Ultrastable triazine-based covalent organic framework with an interlayer hydrogen bonding for supercapacitor applications. *ACS Appl. Mater. Interfaces* **2019**, *11*, 26355–26363.

[2] Xu, P. P.; Liu, J. J.; Yan, P.; Miao, C. X.; Ye, K.; Cheng, K.; Yin, J. L.; Cao, D. X.; Li, K. F.; Wang, G. L. Preparation of porous cadmium sulphide on nickel foam: A novel electrode material with excellent supercapacitor performance. *J. Mater. Chem. A* **2016**, *4*, 4920–4928.

[3] Samireddi, S.; Aishwarya, V.; Shown, I.; Muthusamy, S.; Unni, S. M.; Wong, K. T.; Chen, K. H.; Chen, L. C. Synergistic dual-atom molecular catalyst derived from low-temperature pyrolyzed heterobimetallic macrocycle-N4 corrole complex for oxygen reduction. *Small* **2021**, *17*, 2103823.

[4] Amali, A. J.; Sun, J. K.; Xu, Q. From assembled metal-organic framework nanoparticles to hierarchically porous carbon for electrochemical energy storage. *Chem. Commun.* **2014**, *50*, 1519–1522.

[5] Jiang, M., Yang, J., Ju, J., Zhang W., He, L., Zhang, J., Fu, C., Sun, B. Space-confined synthesis of CoNi nanoalloy in N-doped porous carbon frameworks as efficient oxygen reduction catalyst for neutral and alkaline aluminum-air batteries. *Energy Storage Materials* **2020**, *27*, 96–108.

[6] Pan, Y.; Zhao, Y. X.; Mu, S. J.; Wang, Y.; Jiang, C. M.; Liu, Q. Z.; Fang, Q. R.; Xue, M.; Qiu, S. L. Cation exchanged MOF-derived nitrogen-doped porous carbons for CO_2 capture and supercapacitor electrode materials. *J. Mater. Chem. A* **2017**, *5*, 9544–9552.

[7] Alaş, M. Ö.; Güngör, A.; Genç, R.; Erdem, E. Feeling the power: Robust supercapacitors from nanostructured conductive polymers fostered with Mn^{2+} and carbon dots. *Nanoscale* **2019**, *11*, 12804–12816.

[8] Guo, J. N.; Li, B. J.; Zhang, Q. Y.; Liu, Q. T.; Wang, Z. L.; Zhao, Y. F.; Shui, J. L.; Xiang, Z. H. Highly accessible atomically dispersed Fe-N_x sites electrocatalyst for proton-exchange membrane fuel cell. *Adv. Sci.* **2021**, *8*, 2002249.

[9] Zhang, H. G.; Chung, H. T.; Cullen, D. A.; Wagner, S.; Kramm, U. I.; More, K. L.; Zelenay, P.; Wu, G. High-performance fuel cell cathodes exclusively containing atomically dispersed iron active sites. *Energy Environ. Sci.* **2019**, *12*, 2548–2558.

[10] Zhang, N.; Zhou, T. P.; Chen, M. L.; Feng, H.; Yuan, R. L.; Zhong, C. A.; Yan, W. S.; Tian, Y. C.; Wu, X. J.; Chu, W. S. et al. High-purity pyrrole-type FeN_4 sites as a superior oxygen reduction electrocatalyst. *Energy Environ. Sci.* **2020**, *13*, 111–118.

[11] Huang, Y. P.; Liu, K.; Kan, S. T.; Liu, P. G.; Hao, R.; Liu, W. F.; Wu, Y. F.; Liu, H. T.; Liu, M.; Liu, K. Y. Highly dispersed Fe-N_x active sites on Graphitic-N dominated porous carbon for synergetic catalysis of oxygen reduction reaction. *Carbon* **2021**, *171*, 1–9.

[12] Sarkar, S.; Biswas, A.; Kamboj, N.; Dey, R. S. Unveiling the potential of an Fe bis(terpyridine) complex for precise development of an Fe-N-C electrocatalyst to promote the oxygen reduction reaction. *Inorg. Chem.* **2020**, *59*, 13453–13464.

[13] Jayaramulu, K.; Dubal, D. P.; Nagar, B.; Ranc, V.; Tomanec, O.; Petr, M.; Datta, K. K. R.; Zboril, R.; Gómez-Romero, P.; Fischer, R. A. Ultrathin hierarchical porous carbon nanosheets for high-performance supercapacitors and redox electrolyte energy storage. *Adv. Mater.* **2018**, *30*, 1705789.

[14] Salunkhe, R. R.; Tang, J.; Kamachi, Y.; Nakato, T.; Kim, J. H.; Yamauchi, Y. Asymmetric supercapacitors using 3D nanoporous carbon and cobalt oxide electrodes synthesized from a single metal-organic framework. *ACS Nano* **2015**, *9*, 6288–6296.

[15] Chen, Y. Z.; Zhou, T. F.; Li, L.; Pang, W. K.; He, X. M.; Liu, Y. N.; Guo, Z. P. Interfacial engineering of nickel boride/metaborate and its effect on high energy density asymmetric supercapacitors. *ACS Nano* **2019**, *13*, 9376–9385.

[16] Wang, J.; Polleux, J.; Lim, J.; Dunn, B. Pseudocapacitive contributions to electrochemical energy storage in TiO_2 (anatase) nanoparticles. *J. Phys. Chem. C* **2007**, *111*, 14925–14931.

[17] Feng, C.; Lv, C. P.; Li, Z. Q.; Zhao, H.; Huang, H. H. A porous 2D Ni-MOF material with a high supercapacitive performance. *J. Solid State Chem.* **2018**, *265*, 244–247.

[18] Li, Y. W.; Zhang, W. J.; Li, J.; Ma, H. Y.; Du, H. M.; Li, D. C.; Wang, S. N.; Zhao, J. S.; Dou, J. M.; Xu, L. Q. Fe-MOF-derived efficient ORR/OER bifunctional electrocatalyst for rechargeable Zinc-air batteries. *ACS Appl. Mater. Interfaces* **2020**, *12*, 44710–44719.

[19] Zou, L. L.; Hou, C. C.; Liu, Z.; Pang, H.; Xu, Q. Superlong single-crystal metal-organic framework nanotubes. *J. Am. Chem. Soc.* **2018**, *140*, 15393–15401.

[20] Zhan, G. W.; Zeng, H. C. Synthesis and functionalization of oriented metal-organic-framework nanosheets: Toward a series of 2D catalysts. *Adv. Funct. Mater.* **2016**, *26*, 3268–3281.

[21] Zhang, T.; Manna, K.; Lin, W. B. Metal-organic frameworks stabilize solution-inaccessible cobalt catalysts for highly efficient broad-scope organic transformations. *J. Am. Chem. Soc.* **2016**, *138*, 3241–3249.

[22] Li, Z. X.; Yang, B. L.; Zou, K. Y.; Kong, L. J.; Yue, M. L.; Duan, H. H. Novel porous carbon nanosheet derived from a 2D Cu-MOF: Ultrahigh porosity and excellent performances in the supercapacitor cell. *Carbon* **2019**, *144*, 540–548.

[23] Sahoo, R.; Pham, D. T.; Lee, T. H.; Luu, T. H. T.; Seok, J.; Lee, Y. H. Redox-driven route for widening voltage window in asymmetric supercapacitor. *ACS Nano* **2018**, *12*, 8494–8505.

[24] Mirhosseini, H.; Shamspur, T.; Mostafavi, A.; Sargazi, G. A novel ultrasonic reverse micelle-assisted electrospun efficient route for Eu-MOF and Eu-MOF/CA composite nanofibers: A high performance photocatalytic treatment for removal of BG pollutant. *Environ. Sci. Pollut. Res.* **2021**, *28*, 4317–4328.

[25] Shen, C. H.; Chuang, C. H.; Gu, Y. J.; Ho, W. H.; Song, Y. D.; Chen, Y. C.; Wang, Y. C.; Kung, C. W. Cerium-based metal-organic framework nanocrystals interconnected by carbon nanotubes for boosting electrochemical capacitor performance. *ACS Appl. Mater. Interfaces* **2021**, *13*, 16418–16426.

[26] Vo, T. K.; Nguyen, V. C.; Quang, D. T.; Park, B. J.; Kim, J. Formation of structural defects within UiO-66(Zr)-$(OH)_2$ framework for enhanced CO_2 adsorption using a microwave-assisted continuous-flow tubular reactor. *Microporous Mesoporous Mater.* **2021**, *312*, 110746.

[27] Li, Z. X.; Yang, B. L.; Jiang, Y. F.; Yu, C. Y.; Zhang, L. Metal-directed assembly of five 4-connected MOFs: One-pot syntheses of MOF-derived M_xS_y@C composites for photocatalytic degradation and supercapacitors. *Cryst. Growth Des.* **2018**, *18*, 979–992.

[28] Zou, K. Y.; Zou, Q.; Han, T.; Liu, Y. C.; Wang, J. J.; Zhang, X.; Li, Z. X. Anion-dependent construction of a series of fluorescent coordination polymers based on 1D zinc∩4, 4′-bis(imidazol-1-yl)-biphenyl substrates. *J. Solid State Chem.* **2016**, *235*, 85–92.

[29] Furukawa, H.; Kim, J.; Ockwig, N. W.; O'Keeffe, M.; Yaghi, O. M. Control of vertex geometry, structure dimensionality, functionality, and pore metrics in the reticular synthesis of crystalline metal-organic frameworks and polyhedra. *J. Am. Chem. Soc.* **2008**, *130*, 11650–11661.

[30] Stock, N.; Biswas, S. Synthesis of metal-organic frameworks (MOFs): Routes to various MOF topologies, morphologies, and composites. *Chem. Rev.* **2012**, *112*, 933–969.

[31] Jeon, J. W.; Sharma, R.; Meduri, P.; Arey, B. W.; Schaef, H. T.; Lutkenhaus, J. L.; Lemmon, J. P.; Thallapally, P. K.; Nandasiri, M. I.; McGrail, B. P. et al. *In situ* one-step synthesis of hierarchical nitrogen-doped porous carbon for high-performance supercapacitors. *ACS Appl. Mater. Interfaces* **2014**, *6*, 7214–7222.

[32] Young, C.; Salunkhe, R. R.; Tang, J.; Hu, C. C.; Shahabuddin, M.; Yanmaz, E.; Hossain, S. A.; Kim, J. H.; Yamauchi, Y. Zeolitic imidazolate framework (ZIF-8) derived nanoporous carbon: The effect of carbonization temperature on the supercapacitor performance in an aqueous electrolyte. *Phys. Chem. Chem. Phys.* **2016**, *18*, 29308–29315.

[33] An, C. H.; Wang, Y. J.; Jiao, L. F.; Yuan, H. T. Mesoporous Ni@C hybrids for a high energy aqueous asymmetric supercapacitor device. *J. Mater. Chem. A* **2016**, *4*, 9670–9676.

[34] Liu, X. H.; Zhou, L.; Zhao, Y. Q.; Bian, L.; Feng, X. T.; Pu, Q. S. Hollow, spherical nitrogen-rich porous carbon shells obtained from a porous organic framework for the supercapacitor. *ACS Appl. Mater. Interfaces* **2013**, *5*, 10280–10287.

[35] Şenocak, A.; Tümay, S. O.; Ömeroğlu, İ.; Şanko, V. Crosslinker polycarbazole supported magnetite MOF@CNT hybrid material for synergetic and selective voltammetric determination of adenine and guanine. *J. Electroanal. Chem.* **2022**, *905*, 115963.

[36] Zhang, J.; Li, Z.; Zhang, L.; García Molleja, J.; Wang, D. Y. Bimetallic metal-organic frameworks and Graphene oxide nano-hybrids for enhanced fire retardant epoxy composites: A novel carbonization mechanism. *Carbon* **2019**, *153*, 407–416.

[37] Dědek, I.; Kupka, V.; Jakubec, P.; Šedajová, V.; Jayaramulu, K.; Otyepka, M. Metal-organic framework/conductive polymer hybrid materials for supercapacitors. *Appl. Mater. Today* **2022**, *26*, 101387.

[38] Wei, Y. S.; Zhang, M.; Zou, R. Q.; Xu, Q. Metal-organic framework-based catalysts with single metal sites. *Chem. Rev.* **2020**, *120*, 12089–12174.

[39] Zou, L. L.; Hou, C. C.; Wang, Q. J.; Wei, Y. S.; Liu, Z.; Qin, J. S.; Pang, H.; Xu, Q. A honeycomb-like bulk superstructure of carbon nanosheets for electrocatalysis and energy storage. *Angew. Chem., Int. Ed.* **2020**, *59*, 19627–19632.

[40] Salunkhe, R. R.; Kaneti, Y. V.; Kim, J.; Kim, J. H.; Yamauchi, Y. Nanoarchitectures for metal-organic framework-derived nanoporous carbons toward supercapacitor applications. *Acc. Chem. Res.* **2016**, *49*, 2796–2806.

[41] Shao, Y. L.; El-Kady, M. F.; Sun, J. Y.; Li, Y. G.; Zhang, Q. H.; Zhu, M. F.; Wang, H. Z.; Dunn, B.; Kaner, R. B. Design and mechanisms of asymmetric supercapacitors. *Chem. Rev.* **2018**, *118*, 9233–9280.

[42] Jian, S. L.; Hsiao, L. Y.; Yeh, M. H.; Ho, K. C. Designing a carbon nanotubes-interconnected ZIF-derived cobalt sulfide hybrid nanocage for supercapacitors. *J. Mater. Chem. A* **2019**, *7*, 1479–1490.

[43] Gogotsi, Y.; Penner, R. M. Energy storage in nanomaterials-capacitive, pseudocapacitive, or battery-like? *ACS Nano* **2018**, *12*, 2081–2083.

[44] Díaz, R.; Orcajo, M. G.; Botas, J. A.; Calleja, G.; Palma, J. Co_8-MOF-5 as electrode for supercapacitors. *Mater. Lett.* **2012**, *68*, 126–128.

[45] Liu, X. X.; Shi, C. D.; Zhai, C. W.; Cheng, M. L.; Liu, Q.; Wang, G. X. Cobalt-based layered metal-organic framework as an ultrahigh capacity supercapacitor electrode material. *ACS Appl. Mater. Interfaces* **2016**, *8*, 4585–4591.

[46] Choi, K. M.; Jeong, H. M.; Park, J. H.; Zhang, Y. B.; Kang, J. K.; Yaghi, O. M. Supercapacitors of nanocrystalline metal-organic frameworks. *ACS Nano* **2014**, *8*, 7451–7457.

[47] Yan, Y.; Luo, Y. Q.; Ma, J. Y.; Li, B.; Xue, H. G.; Pang, H. Facile synthesis of vanadium metal-organic frameworks for high-performance supercapacitors. *Small* **2018**, *14*, 1801815.

[48] Jiao, Y.; Pei, J.; Chen, D. H.; Yan, C. H.; Hu, Y. Y.; Zhang, Q.; Chen, G. Mixed-metallic MOF based electrode materials for high performance hybrid supercapacitors. *J. Mater. Chem. A* **2017**, *5*, 1094–1102.

[49] Gholipour-Ranjbar, H.; Soleimani, M.; Naderi, H. R. Application of Ni/Co-based metal-organic frameworks (MOFs) as an advanced electrode material for supercapacitors. *New J. Chem.* **2016**, *40*, 9187–9193.

[50] Gao, W. M.; Chen, D. Z.; Quan, H. Y.; Zou, R.; Wang, W. X.; Luo, X. B.; Guo, L. Fabrication of hierarchical porous metal-organic framework electrode for aqueous asymmetric supercapacitor. *ACS Sustainable Chem. Eng.* **2017**, *5*, 4144–4153.

[51] Sheberla, D.; Bachman, J. C.; Elias, J. S.; Sun, C. J.; Shao-Horn, Y.; Dincă, M. Conductive MOF electrodes for stable supercapacitors with high areal capacitance. *Nat. Mater.* **2017**, *16*, 220–224.

[52] Li, W. H.; Ding, K.; Tian, H. R.; Yao, M. S.; Nath, B.; Deng, W. H.; Wang, Y. B.; Xu, G. Conductive metal-organic framework nanowire array electrodes for high-performance solid-state supercapacitors. *Adv. Funct. Mater.* **2017**, *27*, 1702067.

[53] Ma, J. X.; Li, J.; Guo, R.; Xu, H.; Shi, F.; Dang, L. Q.; Liu, Z. H.; Sun, J.; Lei, Z. B. Direct growth of flake-like metal-organic framework on textile carbon cloth as high-performance supercapacitor electrode. *J. Power Sources* **2019**, *428*, 124–130.

[54] Dai, F. N.; Wang, X. K.; Zheng, S. H.; Sun, J. P.; Huang, Z. D.; Xu, B.; Fan, L. L.; Wang, R. M.; Sun, D. F.; Wu, Z. S. Toward high-performance and flexible all-solid-state micro-supercapacitors: MOF bulk vs. MOF nanosheets. *Chem. Eng. J.* **2021**, *413*, 127520.

[55] Rahmanifar, M. S.; Hesari, H.; Noori, A.; Masoomi, M. Y.; Morsali, A.; Mousavi, M. F. A dual Ni/Co-MOF-reduced graphene oxide nanocomposite as a high performance supercapacitor electrode material. *Electrochim. Acta* **2018**, *275*, 76–86.

[56] Hong, J.; Park, S. J.; Kim, S. Synthesis and electrochemical characterization of nanostructured Ni-Co-MOF/graphene oxide composites as capacitor electrodes. *Electrochim. Acta* **2019**, *311*, 62–71.

[57] Srimuk, P.; Luanwuthi, S.; Krittayavathananon, A.; Sawangphruk, M. Solid-type supercapacitor of reduced graphene oxide-metal organic framework composite coated on carbon fiber paper. *Electrochim. Acta* **2015**, *157*, 69–77.

[58] Saraf, M.; Rajak, R.; Mobin, S. M. A fascinating multitasking Cu-MOF/rGO hybrid for high performance supercapacitors and highly

sensitive and selective electrochemical nitrite sensors. *J. Mater. Chem. A* **2016**, *4*, 16432–16445.

[59] Wang, L.; Feng, X.; Ren, L. T.; Piao, Q. H.; Zhong, J. Q.; Wang, Y. B.; Li, H. W.; Chen, Y. F.; Wang, B. Flexible solid-state supercapacitor based on a metal-organic framework interwoven by electrochemically-deposited PANI. *J. Am. Chem. Soc.* **2015**, *137*, 4920–4923.

[60] Guo, S. N.; Zhu, Y.; Yan, Y. Y.; Min, Y. L.; Fan, J. C.; Xu, Q. J.; Yun, H. (Metal-Organic Framework)-Polyaniline sandwich structure composites as novel hybrid electrode materials for high-performance supercapacitor. *J. Power Sources* **2016**, *316*, 176–182.

[61] Jiao, Y.; Chen, G.; Chen, D. H.; Pei, J.; Hu, Y. Y. Bimetal-organic framework assisted polymerization of pyrrole involving air oxidant to prepare composite electrodes for portable energy storage. *J. Mater. Chem. A* **2017**, *5*, 23744–23752.

[62] Tian, D.; Lu, X. F.; Zhu, Y.; Li, M. X.; Wang, C. Fabrication of two-dimensional metal-organic frameworks on electrospun nanofibers and their derived metal doped carbon nanofibers for an advanced asymmetric supercapacitor with a high energy density. *J. Power Sources* **2019**, *413*, 50–58.

[63] Xu, X. T.; Tang, J.; Qian, H. Y.; Hou, S. J.; Bando, Y.; Hossain, S. A.; Pan, L. K.; Yamauchi, Y. Three-dimensional networked metal-organic frameworks with conductive polypyrrole tubes for flexible supercapacitors. *ACS Appl. Mater. Interfaces* **2017**, *9*, 38737–38744.

[64] Xue, Y. Q.; Zheng, S. S.; Xue, H. G.; Pang, H. Metal-organic framework composites and their electrochemical applications. *J. Mater. Chem. A* **2019**, *7*, 7301–7327.

[65] Xu, Y. X.; Li, Q.; Xue, H. G.; Pang, H. Metal-organic frameworks for direct electrochemical applications. *Coord. Chem. Rev.* **2018**, *376*, 292–318.

[66] Zhou, S. Y.; Kong, X. Y.; Zheng, B.; Huo, F. W.; Strømme, M.; Xu, C. Cellulose nanofiber @ conductive metal-organic frameworks for high-performance flexible supercapacitors. *ACS Nano* **2019**, *13*, 9578–9586.

[67] Song, C.; Yun, J.; Lee, H.; Park, H.; Jeong, Y. R.; Lee, G.; Kim, M. S.; Ha, J. S. A Shape memory high-voltage supercapacitor with asymmetric organic electrolytes for driving an integrated NO_2 gas sensor. *Adv. Funct. Mater.* **2019**, *29*, 1901996.

[68] Wu, X. M.; Huang, B.; Wang, Q. G.; Wang, Y. Wide potential and high energy density for an asymmetric aqueous supercapacitor. *J. Mater. Chem. A* **2019**, *7*, 19017–19025.

[69] Liu, B.; Shioyama, H.; Akita, T.; Xu, Q. Metal-organic framework as a template for porous carbon synthesis. *J. Am. Chem. Soc.* **2008**, *130*, 5390–5391.

[70] Wang, L.; Wei, T.; Sheng, L. Z.; Jiang, L. L.; Wu, X. L.; Zhou, Q. H.; Yuan, B.; Yue, J. M.; Liu, Z.; Fan, Z. J. "Brick-and-mortar" sandwiched porous carbon building constructed by metal-organic framework and graphene: Ultrafast charge/discharge rate up to 2 $V \cdot S^{-1}$ for supercapacitors. *Nano Energy* **2016**, *30*, 84–92.

[71] Salunkhe, R. R.; Kamachi, Y.; Torad, N. L.; Hwang, S. M.; Sun, Z. Q.; Dou, S. X.; Kim, J. H.; Yamauchi, Y. Fabrication of symmetric supercapacitors based on MOF-derived nanoporous carbons. *J. Mater. Chem. A* **2014**, *2*, 19848–19854.

[72] Jiang, H. L.; Liu, B.; Lan, Y. Q.; Kuratani, K.; Akita, T.; Shioyama, H.; Zong, F. Q.; Xu, Q. From metal-organic framework to nanoporous carbon: Toward a very high surface area and hydrogen uptake. *J. Am. Chem. Soc.* **2011**, *133*, 11854–11857.

[73] Xin, L. J.; Chen, R. R.; Liu, Q.; Liu, J. Y.; Li, Z. S.; Li, R. M.; Wang, J. Composites of hierarchical metal-organic framework derived nitrogen-doped porous carbon and interpenetrating 3D hollow carbon spheres from lotus pollen for high-performance supercapacitors. *New J. Chem.* **2017**, *41*, 12835–12842.

[74] Yu, G. L.; Zou, X. Q.; Wang, A. F.; Sun, J.; Zhu, G. S. Generation of bimodal porosity via self-extra porogenes in nanoporous carbons for supercapacitor application. *J. Mater. Chem. A* **2014**, *2*, 15420–15427.

[75] Kim, J.; Young, C.; Lee, J.; Heo, Y. U.; Park, M. S.; Hossain, S. A.; Yamauchi, Y.; Kim, J. H. Nanoarchitecture of MOF-derived nanoporous functional composites for hybrid supercapacitors. *J. Mater. Chem. A* **2017**, *5*, 15065–15072.

[76] Tang, J.; Salunkhe, R. R.; Zhang, H. B.; Malgras, V.; Ahamad, T.; Alshehri, S. M.; Kobayashi, N.; Tominaka, S.; Ide, Y.; Kim, J. H. et al. Bimetallic metal-organic frameworks for controlled catalytic graphitization of nanoporous carbons. *Sci. Rep.* **2016**, *6*, 30295.

[77] Zhu, Q. L.; Pachfule, P.; Strubel, P.; Li, Z. P.; Zou, R. Q.; Liu, Z.; Kaskel, S.; Xu, Q. Fabrication of nitrogen and sulfur co-doped hollow cellular carbon nanocapsules as efficient electrode materials for energy storage. *Energy Storage Mater.* **2018**, *13*, 72–79.

[78] Pachfule, P.; Shinde, D.; Majumder, M.; Xu, Q. Fabrication of carbon nanorods and graphene nanoribbons from a metal-organic framework. *Nat. Chem.* **2016**, *8*, 718–724.

[79] Su, P. P.; Jiang, L.; Zhao, J.; Yan, J. W.; Li, C.; Yang, Q. H. Mesoporous graphitic carbon nanodisks fabricated via catalytic carbonization of coordination polymers. *Chem. Commun.* **2012**, *48*, 8769–8771.

[80] Qu, C.; Jiao, Y.; Zhao, B. T.; Chen, D. C.; Zou, R. Q.; Walton, K. S.; Liu, M. L. Nickel-based pillared MOFs for high-performance supercapacitors: Design, synthesis and stability study. *Nano Energy* **2016**, *26*, 66–73.

[81] Wei, X. J.; Peng, H. R.; Li, Y. H.; Yang, Y. B.; Xiao, S. H.; Peng, L.; Zhang, Y. H.; Xiao, P. *In situ* growth of zeolitic imidazolate framework-67-derived nanoporous carbon@$K_{0.5}Mn_2O_4$ for high-performance 2.4 V aqueous asymmetric supercapacitors. *ChemSusChem* **2018**, *11*, 3167–3174.

[82] Li, X.; Wu, H. J.; Elshahawy, A. M.; Wang, L.; Pennycook, S. J.; Guan, C.; Wang, J. Cactus-like NiCoP/NiCo-OH 3D architecture with tunable composition for high-performance electrochemical capacitors. *Adv. Funct. Mater.* **2018**, *28*, 1800036.

[83] Wang, R. T.; Jin, D. D.; Zhang, Y. B.; Wang, S. J.; Lang, J. W.; Yan, X. B.; Zhang, L. Engineering metal organic framework derived 3D nanostructures for high performance hybrid supercapacitors. *J. Mater. Chem. A* **2017**, *5*, 292–302.

[84] Qu, C.; Liang, Z. B.; Jiao, Y.; Zhao, B. T.; Zhu, B. J.; Dang, D.; Dai, S. G.; Chen, Y.; Zou, R. Q.; Liu, M. L. "One-for-all" strategy in fast energy storage: Production of pillared MOF nanorod-templated positive/negative electrodes for the application of high-performance hybrid supercapacitor. *Small* **2018**, *14*, 1800285.

[85] Gu, Y. Y.; Miao, L.; Yin, Y.; Liu, M. X.; Gan, L. H.; Li, L. C. Highly N/O co-doped ultramicroporous carbons derived from nonporous metal-organic framework for high performance supercapacitors. *Chin. Chem. Lett.* **2021**, *32*, 1491–1496.

[86] Gong, Y. J.; Chen, R. Y.; Xu, H. Y.; Yu, C. Y.; Zhao, X.; Sun, Y.; Hui, Z. Y.; Zhou, J. Y.; An, J. N.; Du, Z. Z. et al. Polarity-assisted formation of hollow-frame sheathed nitrogen-doped nanofibrous carbon for supercapacitors. *Nanoscale* **2019**, *11*, 2492–2500.

[87] Zhang, W.; Li, R.; Zheng, H.; Bao, J. S.; Tang, Y. J.; Zhou, K. Laser-assisted printing of electrodes using metal-organic frameworks for micro-supercapacitors. *Adv. Funct. Mater.* **2021**, *31*, 2009057.

[88] Tang, A. C.; Wan, C. B.; Hu, X. Y.; Ju, X. Metal-organic framework-derived Ni/ZnO nano-sponges with delicate surface vacancies as anode materials for high-performance supercapacitors. *Nano Res.* **2021**, *14*, 4063–4072.

[89] Meng, F. L.; Fang, Z. G.; Li, Z. X.; Xu, W. W.; Wang, M. J.; Liu, Y. P.; Zhang, J.; Wang, W. R.; Zhao, D. Y.; Guo, X. H. Porous Co_3O_4 materials prepared by solid-state thermolysis of a novel Co-MOF crystal and their superior energy storage performances for supercapacitors. *J. Mater. Chem. A* **2013**, *1*, 7235–7241.

[90] Qu, C.; Zhao, B. T.; Jiao, Y.; Chen, D. C.; Dai, S. G.; Deglee, B. M.; Chen, Y.; Walton, K. S.; Zou, R. Q.; Liu, M. L. Functionalized bimetallic hydroxides derived from metal-organic frameworks for high-performance hybrid supercapacitor with exceptional cycling stability. *ACS Energy Lett.* **2017**, *2*, 1263–1269.

[91] Wang, P. Y.; Li, Y. N.; Li, S. D.; Liao, X. Q.; Sun, S. M. Water-promoted zeolitic imidazolate framework-67 transformation to Ni-Co layered double hydroxide hollow microsphere for supercapacitor electrode material. *J. Mater. Sci.: Mater. Electron.* **2017**, *28*, 9221–9227.

[92] Hu, H.; Guan, B. Y.; Lou, X. W. Construction of complex CoS hollow structures with enhanced electrochemical properties for

hybrid supercapacitors. *Chem* **2016**, *1*, 102–113.
[93] Ma, X.; Zhang, L.; Xu, G. C.; Zhang, C. Y.; Song, H. J.; He, Y. T.; Zhang, C.; Jia, D. Z. Facile synthesis of NiS hierarchical hollow cubes via Ni formate frameworks for high performance supercapacitors. *Chem. Eng. J.* **2017**, *320*, 22–28.
[94] Liang, Z. B.; Qu, C.; Zhou, W. Y.; Zhao, R.; Zhang, H.; Zhu, B. J.; Guo, W. H.; Meng, W.; Wu, Y. X.; Aftab, W. et al. Synergistic effect of Co-Ni hybrid phosphide nanocages for ultrahigh capacity fast energy storage. *Adv. Sci.* **2019**, *6*, 1802005.
[95] Lai, F. L.; Feng, J. R.; Heil, T.; Tian, Z. H.; Schmidt, J.; Wang, G. C.; Oschatz, M. Partially delocalized charge in Fe-doped $NiCo_2S_4$ nanosheet-mesoporous carbon-composites for high-voltage supercapacitors. *J. Mater. Chem. A* **2019**, *7*, 19342–19347.
[96] Yu, X.; Yu, J. L.; Fautrelle, Y.; Gagnoud, A.; Ren, Z. M.; Lu, X. G.; Li, X. Strong magnetic field-dual-assisted fabrication of heterogeneous sulfide-based hollow nanochain electrodes for high-rate supercapacitors. *J. Mater. Chem. A* **2019**, *7*, 19733–19744.
[97] Xia, Q. X.; Shinde, N. M.; Yun, J. M.; Zhang, T. F.; Mane, R. S.; Mathur, S.; Kim, K. H. Bismuth oxychloride/MXene symmetric supercapacitor with high volumetric energy density. *Electrochim. Acta* **2018**, *271*, 351–360.
[98] Yi, H.; Wang, H. W.; Jing, Y. T.; Peng, T. Q.; Wang, X. F. Asymmetric supercapacitors based on carbon nanotubes@NiO ultrathin nanosheets core–shell composites and MOF-derived porous carbon polyhedrons with super-long cycle life. *J. Power Sources* **2015**, *285*, 281–290.
[99] Ji, D.; Zhou, H.; Zhang, J.; Dan, Y. Y.; Yang, H. X.; Yuan, A. H. Facile synthesis of a metal-organic framework-derived Mn_2O_3 nanowire coated three-dimensional graphene network for high-performance free-standing supercapacitor electrodes. *J. Mater. Chem. A* **2016**, *4*, 8283–8290.
[100] Wang, Y. C.; Li, W. B.; Zhao, L.; Xu, B. Q. MOF-derived binary mixed metal/metal oxide @carbon nanoporous materials and their novel supercapacitive performances. *Phys. Chem. Chem. Phys.* **2016**, *18*, 17941–17948.
[101] Tong, M. Y.; Liu, S. W.; Zhang, X.; Wu, T. X.; Zhang, H. M.; Wang, G. Z.; Zhang, Y. X.; Zhu, X. G.; Zhao, H. J. Two-dimensional CoNi nanoparticles@S,N-doped carbon composites derived from S, N-containing Co/Ni MOFs for high performance supercapacitors. *J. Mater. Chem. A* **2017**, *5*, 9873–9881.
[102] Cai, C. L.; Zou, Y. J.; Xiang, C. L.; Chu, H. L.; Qiu, S. J.; Sui, Q. L.; Xu, F.; Sun, L. X.; Shah, A. Broccoli-like porous carbon nitride from ZIF-8 and melamine for high performance supercapacitors. *Appl. Surf. Sci.* **2018**, *440*, 47–54.
[103] Liu, G. J.; Wang, B.; Wang, L.; Yuan, Y. H.; Wang, D. L. A facile hydrothermal synthesis of a reduced graphene oxide modified cobalt disulfide composite electrode for high-performance supercapacitors. *RSC Adv.* **2016**, *6*, 7129–7138.
[104] Song, Z. X.; Zhu, Y. N.; Liu, H. S.; Banis, M. N.; Zhang, L.; Li, J. J.; Doyle-Davis, K.; Li, R. Y.; Sham, T. K.; Yang, L. J. et al. Engineering the low coordinated Pt single atom to achieve the superior electrocatalytic performance toward oxygen reduction. *Small* **2020**, *16*, 2003096.
[105] Shao, C. F.; Zhuang, S. G.; Zhang, H. C.; Jiang, Q. K.; Xu, X. Y.; Ye, J. S.; Li, B. T.; Wang, X. J. Enhancement of mass transport for oxygen reduction reaction using petal-like porous Fe-NC nanosheet. *Small* **2021**, *17*, 2006178.
[106] Lu, Z. Y.; Wang, B.; Hu, Y. F.; Liu, W.; Zhao, Y. F.; Yang, R. O.; Li, Z. P.; Luo, J.; Chi, B.; Jiang, Z. et al. An isolated zinc-cobalt atomic pair for highly active and durable oxygen reduction. *Angew. Chem., Int. Ed.* **2019**, *58*, 2622–2626.
[107] Wang, Y.; Zheng, X. B.; Wang, D. S. Design concept for electrocatalysts. *Nano Res.* **2022**, *15*, 1730–1752.
[108] Usov, P. M.; Huffman, B.; Epley, C. C.; Kessinger, M. C.; Zhu, J.; Maza, W. A.; Morris, A. J. Study of electrocatalytic properties of metal-organic framework PCN-223 for the oxygen reduction reaction. *ACS Appl. Mater. Interfaces* **2017**, *9*, 33539–33543.
[109] Miner, E. M.; Fukushima, T.; Sheberla, D.; Sun, L.; Surendranath, Y.; Dincă, M. Electrochemical oxygen reduction catalysed by Ni_3(Hexaiminotriphenylene)$_2$. *Nat. Commun.* **2016**, *7*, 10942.
[110] Jiang, M.; Li, L. J.; Zhu, D. D.; Zhang, H. Y.; Zhao, X. B. Oxygen reduction in the nanocage of metal-organic frameworks with an electron transfer mediator. *J. Mater. Chem. A* **2014**, *2*, 5323–5329.
[111] Sohrabi, S.; Dehghanpour, S.; Ghalkhani, M. Three-dimensional metal-organic framework graphene nanocomposite as a highly efficient and stable electrocatalyst for the oxygen reduction reaction in acidic media. *ChemCatChem* **2016**, *8*, 2356–2366.
[112] Jahan, M.; Bao, Q. L.; Loh, K. P. Electrocatalytically active graphene–porphyrin MOF composite for oxygen reduction reaction. *J. Am. Chem. Soc.* **2012**, *134*, 6707–6713.
[113] Guo, J. N.; Li, Y.; Cheng, Y. H.; Dai, L. M.; Xiang, Z. H. Highly efficient oxygen reduction reaction electrocatalysts synthesized under nanospace confinement of metal-organic framework. *ACS Nano* **2017**, *11*, 8379–8386.
[114] Zhong, H. X.; Ly, K. H.; Wang, M. C.; Krupskaya, Y.; Han, X. C.; Zhang, J. C.; Zhang, J.; Kataev, V.; Büchner, B.; Weidinger, I. M. et al. A phthalocyanine-based layered two-dimensional conjugated metal-organic framework as a highly efficient electrocatalyst for the oxygen reduction reaction. *Angew. Chem., Int. Ed.* **2019**, *58*, 10677–10682.
[115] He, X. B.; Yin, F. X.; Li, G. R. A Co/metal-organic-framework bifunctional electrocatalyst: The effect of the surface cobalt oxidation state on oxygen evolution/reduction reactions in an alkaline electrolyte. *Int. J. Hydrogen Energy* **2015**, *40*, 9713–9722.
[116] Fu, S. F.; Zhu, C. Z.; Song, J. H.; Du, D.; Lin, Y. H. Metal-organic framework-derived non-precious metal nanocatalysts for oxygen reduction reaction. *Adv. Energy Mater.* **2017**, *7*, 1700363.
[117] Delaporte, N.; Rivard, E.; Natarajan, S. K.; Benard, P.; Trudeau, M. L.; Zaghib, K. Synthesis and performance of MOF-based non-noble metal catalysts for the oxygen reduction reaction in proton-exchange membrane fuel cells: A review. *Nanomaterials* **2020**, *10*, 1947.
[118] Sohrabi, S.; Ghalkhani, M. Metal-organic frameworks as electro-catalysts for oxygen reduction reaction in electrochemical technologies. *J. Electron. Mater.* **2019**, *48*, 4127–4137.
[119] Lyu, X.; Jia, Y.; Mao, X.; Li, D. H.; Li, G.; Zhuang, L. Z.; Wang, X.; Yang, D. J.; Wang, Q.; Du, A. J. et al. Gradient-concentration design of stable core–shell nanostructure for acidic oxygen reduction electrocatalysis. *Adv. Mater.* **2020**, *32*, 2003493.
[120] Wang, Y. Q.; Tao, L.; Xiao, Z. H.; Chen, R.; Jiang, Z. Q.; Wang, S. Y. 3D carbon electrocatalysts *in situ* constructed by defect-rich nanosheets and polyhedrons from NaCl-sealed zeolitic imidazolate frameworks. *Adv. Funct. Mater.* **2018**, *28*, 1705356.
[121] Chai, L. L.; Zhang, L. J.; Wang, X.; Xu, L. Q.; Han, C.; Li, T. T.; Hu, Y.; Qian, J. J.; Huang, S. M. Bottom-up synthesis of MOF-derived hollow N-doped carbon materials for enhanced ORR performance. *Carbon* **2019**, *146*, 248–256.
[122] Zhang, L. J.; Wang, X. Y.; Wang, R. H.; Hong, M. C. Structural evolution from metal-organic framework to hybrids of nitrogen-doped porous carbon and carbon nanotubes for enhanced oxygen reduction activity. *Chem. Mater.* **2015**, *27*, 7610–7618.
[123] Huang, P. M.; Li, H. D.; Huang, X. Y.; Chen, D. Y. Multiheteroatom-doped porous carbon catalyst for oxygen reduction reaction prepared using 3D network of ZIF-8/polymeric nanofiber as a facile-doping template. *ACS Appl. Mater. Interfaces* **2017**, *9*, 21083–21088.
[124] Liu, M. L.; Zhao, Z. P.; Duan, X. F.; Huang, Y. Nanoscale structure design for high-performance Pt-based ORR catalysts. *Adv. Mater.* **2019**, *31*, 1802234.
[125] Li, W. Y.; Zou, S. Z. PtNi nanoparticles encapsulated in few carbon layers as high-performance catalysts for oxygen reduction reaction. *ACS Appl. Energy Mater.* **2019**, *2*, 2769–2778.
[126] Wang, X. X.; Hwang, S.; Pan, Y. T.; Chen, K. T.; He, Y. H.; Karakalos, S.; Zhang, H. G.; Spendelow, J. S.; Su, D.; Wu, G. Ordered Pt_3Co intermetallic nanoparticles derived from metal-organic frameworks for oxygen reduction. *Nano Lett.* **2018**, *18*, 4163–4171.
[127] Xia, Z. X.; Fang, J.; Zhang, X. M.; Fan, L. P.; Barlow, A. J.; Lin, T.; Wang, S. L.; Wallace, G. G.; Sun, G. Q.; Wang, X. G. Pt nanoparticles embedded metal-organic framework nanosheets: A

synergistic strategy towards bifunctional oxygen electrocatalysis. *Appl. Catal. B Environ.* **2019**, *245*, 389–398.

[128] Du, C.; Gao, X. H.; Cheng, C. F.; Zhuang, Z. H.; Li, X. K.; Chen, W. Metal organic framework for the fabrication of mutually interacted Pt-CeO_2-C ternary nanostructure: Advanced electrocatalyst for oxygen reduction reaction. *Electrochim. Acta* **2018**, *266*, 348–356.

[129] Li, H. C.; Zhang, Y. J.; Hu, X.; Liu, W. J.; Chen, J. J.; Yu, H. Q. Metal-organic framework templated Pd@PdO-Co_3O_4 nanocubes as an efficient bifunctional oxygen electrocatalyst. *Adv. Energy Mater.* **2018**, *8*, 1702734.

[130] Liang, Z. B.; Qu, C.; Xia, D. G.; Zou, R. Q.; Xu, Q. Atomically dispersed metal sites in MOF-based materials for electrocatalytic and photocatalytic energy conversion. *Angew. Chem., Int. Ed.* **2018**, *57*, 9604–9633.

[131] Zhu, P.; Xiong, X.; Wang, D. S. Regulations of active moiety in single atom catalysts for electrochemical hydrogen evolution reaction. *Nano Res*., in press, https://doi.org/10.1007/s12274-022-4265-y.

[132] Xu, H.; Wang, D.; Yang, P. X.; Liu, A. M.; Li, R. P.; Li, Y.; Xiao, L. H.; Ren, X. F.; Zhang, J. Q.; An, M. Z. Atomically dispersed M-N-C catalysts for the oxygen reduction reaction. *J. Mater. Chem. A* **2020**, *8*, 23187–23201.

[133] Gawande, M. B.; Ariga, K.; Yamauchi, Y. Single-atom catalysts. *Small* **2021**, *17*, 2101584.

[134] Han, A. L.; Wang, X. J.; Tang, K.; Zhang, Z. D.; Ye, C. L.; Kong, K. J.; Hu, H. B.; Zheng, L. R.; Jiang, P.; Zhao, C. X. et al. An adjacent atomic platinum site enables single-atom iron with high oxygen reduction reaction performance. *Angew. Chem., Int. Ed.* **2021**, *60*, 19262–19271.

[135] Chen, Y. J.; Ji, S. F.; Wang, Y. G.; Dong, J. C.; Chen, W. X.; Li, Z.; Shen, R. A.; Zheng, L. R.; Zhuang, Z. B.; Wang, D. S. et al. Isolated single iron atoms anchored on N-doped porous carbon as an efficient electrocatalyst for the oxygen reduction reaction. *Angew. Chem., Int. Ed.* **2017**, *56*, 6937–6941.

[136] Zhang, H. G.; Hwang, S.; Wang, M. Y.; Feng, Z. X.; Karakalos, S.; Luo, L. L.; Qiao, Z.; Xie, X. H.; Wang, C. M.; Su, D. et al. Single atomic iron catalysts for oxygen reduction in acidic media: Particle size control and thermal activation. *J. Am. Chem. Soc.* **2017**, *139*, 14143–14149.

[137] Ye, H.; Li, L. J.; Liu, D. D.; Fu, Q. J.; Zhang, F. Z.; Dai, P. C.; Gu, X.; Zhao, X. B. Sustained-release method for the directed synthesis of ZIF-derived ultrafine Co-N-C ORR catalysts with embedded Co quantum dots. *ACS Appl. Mater. Interfaces* **2020**, *12*, 57847–57858.

[138] Chen, M. J.; Li, X.; Yang, F.; Li, B. Y.; Stracensky, T.; Karakalos, S.; Mukerjee, S.; Jia, Q. Y.; Su, D.; Wang, G. F. et al. Atomically dispersed MnN_4 catalysts via environmentally benign aqueous synthesis for oxygen reduction: Mechanistic understanding of activity and stability improvements. *ACS Catal.* **2020**, *10*, 10523–10534.

[139] Wang, J.; Huang, Z. Q.; Liu, W.; Chang, C. R.; Tang, H. L.; Li, Z. J.; Chen, W. X.; Jia, C. J.; Yao, T.; Wei, S. Q. et al. Design of N-coordinated dual-metal sites: A stable and active Pt-free catalyst for acidic oxygen reduction reaction. *J. Am. Chem. Soc.* **2017**, *139*, 17281–17284.

[140] Lu, X. F.; Chen, Y.; Wang, S. B.; Gao, S. Y.; Lou, X. W. Interfacing manganese oxide and cobalt in porous graphitic carbon polyhedrons boosts oxygen electrocatalysis for Zn-air batteries. *Adv. Mater.* **2019**, *31*, 1902339.

[141] Ding, D. N.; Shen, K.; Chen, X. D.; Chen, H. R.; Chen, J. Y.; Fan, T.; Wu, R. F.; Li, Y. W. Multi-level architecture optimization of MOF-templated Co-based nanoparticles embedded in hollow N-doped carbon polyhedra for efficient OER and ORR. *ACS Catal.* **2018**, *8*, 7879–7888.

[142] Guan, B. Y.; Yu, L.; Lou, X. W. A dual-metal-organic-framework derived electrocatalyst for oxygen reduction. *Energy Environ. Sci.* **2016**, *9*, 3092–3096.

[143] Mao, J. J.; Yang, L. F.; Yu, P.; Wei, X. W.; Mao, L. Q. Electrocatalytic four-electron reduction of oxygen with copper (II)-based metal-organic frameworks. *Electrochem. Commun.* **2012**, *19*, 29–31.

[144] Cho, K.; Han, S. H.; Suh, M. P. Copper-organic framework fabricated with CuS nanoparticles: Synthesis, electrical conductivity, and electrocatalytic activities for oxygen reduction reaction. *Angew. Chem., Int. Ed.* **2016**, *128*, 15527–15531.

[145] Ma, X.; Zhao, X.; Sun, J.; Li, D. H.; Yang, X. R. A versatile strategy to fabricate MOFs/carbon material integrations and their derivatives for enhanced electrocatalysis. *RSC Adv.* **2016**, *6*, 7728–7735.

[146] Fu, Y. A.; Huang, Y.; Xiang, Z. H.; Liu, G. Q.; Cao, D. P. Phosphorous-nitrogen-codoped carbon materials derived from metal-organic frameworks as efficient electrocatalysts for oxygen reduction reactions. *Eur. J. Inorg. Chem.* **2016**, *2016*, 2100–2105.

[147] Hu, H.; Han, L.; Yu, M. Z.; Wang, Z. Y.; Lou, X. W. Metal-organic-framework-engaged formation of Co nanoparticle-embedded carbon@Co_9S_8 double-shelled nanocages for efficient oxygen reduction. *Energy Environ. Sci.* **2016**, *9*, 107–111.

[148] Aijaz, A.; Masa, J.; Rösler, C.; Xia, W.; Weide, P.; Botz, A. J. R.; Fischer, R. A.; Schuhmann, W.; Muhler, M. Co@Co_3O_4 encapsulated in carbon nanotube-grafted nitrogen-doped carbon polyhedra as an advanced bifunctional oxygen electrode. *Angew. Chem., Int. Ed.* **2016**, *55*, 4087–4091.

[149] Ma, S. Q.; Goenaga, G. A.; Call, A. V; Liu, D. J. Cobalt imidazolate framework as precursor for oxygen reduction reaction electrocatalysts. *Chem. —Eur. J.* **2011**, *17*, 2063–2067.

[150] You, B.; Jiang, N.; Sheng, M. L.; Drisdell, W. S.; Yano, J.; Sun, Y. J. Bimetal-organic framework self-adjusted synthesis of support-free nonprecious electrocatalysts for efficient oxygen reduction. *ACS Catal.* **2015**, *5*, 7068–7076.

[151] Xiao, M. L.; Chen, Y. T.; Zhu, J. B.; Zhang, H.; Zhao, X.; Gao, L. Q.; Wang, X.; Zhao, J.; Ge, J. J.; Jiang, Z. et al. Climbing the apex of the ORR volcano plot via binuclear site construction: Electronic and geometric engineering. *J. Am. Chem. Soc.* **2019**, *141*, 17763–17770.

[152] Yang, G. G.; Zhu, J. W.; Yuan, P. F.; Hu, Y. F.; Qu, G.; Lu, B. A.; Xue, X. Y.; Yin, H. B.; Cheng, W. Z.; Cheng, J. Q. et al. Regulating Fe-spin state by atomically dispersed Mn-N in Fe-N-C catalysts with high oxygen reduction activity. *Nat. Commun.* **2021**, *12*, 1734.

[153] Zhang, S.; Xue, H.; Li, W. L.; Sun, J.; Guo, N. K.; Song, T. S.; Dong, H. L.; Zhang, J. W.; Ge, X.; Zhang, W. et al. Constructing precise coordination of nickel active sites on hierarchical porous carbon framework for superior oxygen reduction. *Small* **2021**, *17*, 2102125.

[154] Li, J. Z.; Chen, M. J.; Cullen, D. A.; Hwang, S.; Wang, M. Y.; Li, B. Y.; Liu, K. X.; Karakalos, S.; Lucero, M.; Zhang, H. G. et al. Atomically dispersed manganese catalysts for oxygen reduction in proton-exchange membrane fuel cells. *Nat. Catal.* **2018**, *1*, 935–945.